Predicting Impact Damage for Carbon Composite Propeller Certification

Master Thesis

Kasper Sijmons
4351088

Delft University of Technology

TU Delft

PAL-V

Predicting Impact Damage for Carbon Composite Propeller Certification

Master Thesis

by

Kasper Sijmons
4351088

to obtain the degree of Master of Science
at the Delft University of Technology,
to be defended publicly on Friday October 6, 2023 at 13:00.

Student number:	4351088	
Project duration:	October 10, 2022 – October 6, 2023	
Thesis committee:	Dr. ir. R. C. Alderliesten,	TU Delft, chair
	Dr. ir. J. M. J. F. van Campen,	TU Delft, supervisor
	Dr. ir. J. A. Pascoe,	TU Delft
	Ir. G. H. A. van Gool,	PAL-V

This thesis is confidential and cannot be made public until October 6, 2025.

Cover: The PAL-V Liberty. image credit: PAL-V

An electronic version of this thesis is available at `http://repository.tudelft.nl/`.

TU Delft

Preface

The document you are reading now is the final work that was performed to fulfil the master thesis requirements of the Aerospace Structures and Materials department at the Delft University of Technology.

First and foremost, I would like to thank my supervisors at the TU Delft for their excellent guidance, advice and support. It was great to see that Julien van Campen was genuinely enthusiastic about the thesis opportunity that PAL-V offered me. When it became clear that this project would involve certification, John-Alan Pascoe was brought on board who shared the same enthusiasm. The sincere interest in my progress and results during the biweekly meetings kept me motivated and assured me that I was on the right track.
I would also like to thank my supervisor and all the other people that helped me at PAL-V. Guido van Gool provided me with the connections I needed within PAL-V and with critical feedback on my work. I hope this research can provide some assistance in the upcoming certification work done on the PAL-V Liberty.

The completion of my master's degree would not have been possible without the emotional and financial support of my parents. Although it took me a lot longer than expected, draining their bank account in the process, they never let me down.

Finally I would like to thank Timo, Thomas and the other people who supported me these last weeks when performing the challenging task of finishing this monumental document.

Kasper Sijmons
4351088
Delft, September 2023

Summary

During this research, a new approach to predict impact damage was evaluated using the PAL-V Liberty's propeller blade as the test subject. The purpose of this research was to provide a simple method for impact damage prediction which will support the certification activities of the PAL-V propeller.

This method involves conducting a threat assessment, a Probability of Detection analysis, executing ASTM D7136 impact and quasi-static tests on coupon samples and conducting quasi-static tests on the propeller blade itself. The results from these tests were used to create a two-mass model which can predict the contact force during a propeller impact event. This model was validated using impact test on the propeller blade.

The study conducted a series of ASTM D7136 impact tests and quasi-static tests on coupons, revealing that the coupons exhibited greater load-bearing capacity under impact loading compared to quasi-static loading. These tests also showed that the coupons have an increased stiffness when subjected to impact loading, requiring a multiplication factor of 1.47 to align their stiffness with quasi-static conditions.

The research also involved determining boundary conditions for propeller tests, which led to the development of a custom clamping mechanism. During the quasi-static tests, the differences in stiffness between coupon and propeller tests were identified. These coefficients served as the basis for a predictive model involving a two-mass, spring and damper system, with parameters derived from coupon tests and the propeller quasi-static tests. After performing the validation impact tests on the propeller blade, it was determined that this model successfully predicted contact forces within 13% of actual test values.

The research demonstrated the potential to predict impact energy requirements for barely visible impact damage, without the use of FEA. The model's accuracy, while it can be improved, is sufficient to predict impact events effectively, offering a simpler alternative to complex FEA models.

Contents

List of Figures

List of Tables

Nomenclature

Abbreviations

Abbreviation	Definition
AMC	Acceptable Means of Compliance
ASTM	American Society for Testing and Materials
BVID	Barely Visible Impact Damage
CAI	Compression After Impact
CBS	Centraal Bureau voor de Statistiek
CS	Certification Specification
CVID	Clearly Visible Impact Damage
DT	Detectability Threshold
FEA	Finite Element Analysis
FEM	Finite Element Method
FOD	Foreign Object Debris
ISO	International Standardization Organization
LVI	Low Velocity Impact
NDE	Non-Destructive Evaluation
NLR	Nederlands Lucht- en Ruimtevaartcentrum
PoD	Probability of Detection
RPM	Revolutions Per Minute
SC	Special Condition
SD	Standard Deviation
VFR	Visual Flight Rules
VID	Visible Impact Damage

Symbols

Symbol	Definition	Unit
C_c	Contact Damping	[Ns/m]
C_p	Propeller Damping	[Ns/m]
dt	Time Interval	[s]
E	Modulus of Elasticity	[Pa]
F	Force	[N]
J_i	Impulse	[Ns]
k_α	Contact Stiffness	[N/m]
k_β	Boundary Stiffness	[N/m]
k_c	Contact Stiffness (propeller)	[N/m]
k_m	Membrane Stiffness	[N/m]
k_p	Propeller Stiffness	[N/m]
k_s	Shear Stiffness	[N/m]
M	Impactor Mass	[kg]
M_p	Local Plate Mass	[kg]
p	Momentum	[Ns]
t	Time	[s]
ΔV	Velocity Change	[m/s]
$\mu\epsilon$	Microstrain	[-]

1

Introduction

Carbon composite materials have gained significant attention in aerospace applications due to their high strength-to-weight ratio and excellent fatigue resistance. These materials have been used extensively in the construction of aircraft components, including propellers. However, the impact damage resistance of composite structural parts has been a challenging issue because impact damage forms a higher threat to composite parts compared to conventional metal parts [1]. The main reason is the fact that impact damage in carbon composites is not necessarily visible from the outside while already causing significant loss of structural properties. This type of damage is called Barely Visible Impact Damage (BVID) [1].

PAL-V is currently in development of the PAL-V Liberty. This will be the first fully certified flying car in the world. This vehicle will be able to function in different modes. In the flying mode the vehicle will function as a gyroplane. This is a form of rotorcraft in which the rotor system is not powered during flight. The use of a rotor instead of wings for the PAL-V Liberty means there are no large wings that take up a lot of space. Creating a gyroplane instead of a helicopter means the PAL-V Liberty will have the space advantage of the compact rotor system without adding the complexity of a helicopter rotor system. The second mode is drive mode. In this mode the PAL-V Liberty will drive like a normal road car. This means the rotor system will be folded and the tail will be retracted. The suspension will also be lowered and therefore the propeller needs to be folded.

The very specific requirements of this vehicle mean that no existing propeller is suited for the PAL-V Liberty which leads to the in-house development of a lightweight folding propeller. Because a carbon composite propeller can offer 25-30% weight saved when comparing to an aluminium propeller [2], it is the obvious material of choice for the PAL-V Liberty propeller. The in-house development of a carbon composite propeller blade means that PAL-V will have to go through the certification process. This process involves proving the impact damage resistance of the propeller which involves proving that BVID will not be a structural hazard on the PAL-V Liberty propeller. This includes performing fatigue testing on a propeller blade with BVID present.

In structural engineering there currently exists a trend towards finite element modelling and complex computations. Not all companies have the resources to use advanced modeling software. PAL-V is currently growing but nowhere near the size of larger aircraft manufacturers like Boeing or Airbus. For PAL-V performing finite element modelling on impact damage events is currently not available. That is why in this thesis an approach will be used which avoids the use of this software and focuses on physical testing.

The goal of this research was to develop a method to inflict BVID to a carbon composite propeller blade which can be used for certification while minimizing the resources required.

First, in a literature review in chapter 2, the state of the art in the field of impact damage on composites was explored. This chapter explores the theory and mechanics of impact damage, certification requirements and impact damage predictions. From this review, research questions were formed in section 2.6. How these research questions were answered is explained in chapter 3 where a method of predicting impact damage is proposed. This method was executed on the PAL-V Liberty propeller blade to explore the viability of this approach.

Chapter 4 and chapter 5 explain the requirements and location for BVID for certification. In chapter 6 impact tests and quasi-static tests were performed to characterize the material and layup used for the PAL-V Propeller. The structural response of the propeller blade was determined by performing quasi-static tests on the propeller blade. This is explained in chapter 7.

From these tests a prediction model was made which is presented in chapter 8. This model was validated using impact testing on the propeller in chapter 9. The conclusions and recommendation from this research can be found in chapter 10 and chapter 11

2

Literature Review

A large collection of research has already been done on impact damage and certification. This review will present the current understanding of impact damage and summarize the relevant literature which will support the research questions and method for this thesis. The goal for this research, stated in chapter 1, mentions inflicting BVID on a carbon composite propeller for certification. This literature review will explore what BVID is, how it is created and how it will be used for certification. In section 2.2 it is explored what is necessary to certify a composite structure and what BVID is. In section 2.3 the mechanisms at play when impact damage is created is reviewed. A review of methods to determine the impact events that inflict a certain impact damage will be given in section 2.4.

2.1. What is Impact Damage

Impact in mechanics is defined as the collision between structures [3]. Impact damage is therefore the damage resulting from one object hitting another. In aerospace engineering, this impact is the impact of an external object hitting the aircraft structure. The object can be referred to as the impactor and the aircraft structure as the target. The target is usually assumed stationary with the impactor having an impact velocity.

Impact damage refers to all damage resulting from this impact event. In metals, this damage is often clearly visible from the outside. Dents, cracks or tears in the metal structure are visible by inspection from the exterior of the metal [4]. In composites, this is not always the case. The impact damage can be dents or broken fibers visible from the outside but can also be damage inside the composite part like delaminations or matrix cracks [5].

2.2. Certification

One of the goals of this research was to support the certification work of the PAL-V propeller. This section will explore what is needed to certify a carbon composite propeller and what roll impact damage plays in this process. The certification specification that is used for the PAL-V Liberty propeller is CS-27 [6] with special condition GYRO [7]. This certification specification is meant for small rotercraft. The special condition GYRO was created specifically for PAL-V to certify an autogyro aircraft with road driving capabilities. The propeller on the PAL-V Liberty will be certified according to the certification specification CS-P [8] for propellers.

Certification Basis

The PAL-V liberty will be certified based on the Certification Specifications for Propellers or CS-P (Amendment 2) by EASA [8]. In these certification specifications it is only stated that the structural integrity during the entire propeller operating life must be established while taking into account the environmental effects. These environmental effects include impact damage events. CS-P [8] does not provide a method or specific requirements regarding impact damage in composites even though this is a complex certification issue.

EASA has recognised that impact damage is a complicated issue in composites and has published AMC-20-29 [9]. This is a document providing acceptable means of compliance for the certification

of composite aircraft structures. The goal of this document was to increase the aviation safety by standardising the certification methods used. The methods provided in AMC 20-29 [9] are not the only ways in which a composite component can be certified but can provide a guide for companies to ensure certification success. These methods will also be used by PAL-V, and in this thesis, to determine a certification strategy for the propeller.

2.2.1. Damage Classification

In the introdution in chapter 1 it was explained that the difficulty when dealing with impact damage in a composite structure is the possibility that a composite components can already be structurally compromised by an impact event without a visible indication on the outside of the part. This means that, for certification, it was useful to categorize impact damages based on detectability. The detectability determines if and after how long impact damage is detected and thus how long it can be present in a composite component before repair or replacement. This information was then used to determine the acceptable residual strength for certain damage categories.

In AMC-20-29 [9], impact damage is split into 5 categories. In Figure 2.1 these categories are shown. These 5 categories are taken from AMC-20-29 [9] and are also used in the Composites Materials Handbook [1]. The 5 categories are explained below.

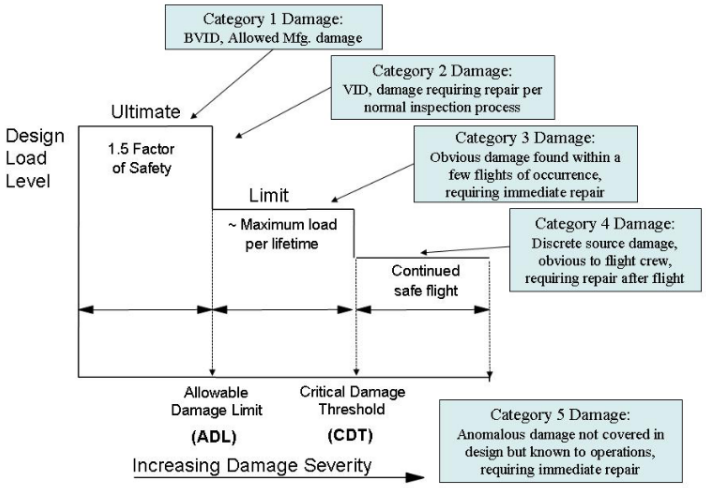

Figure 2.1: Damage Categories based on Detectability [9]

Category 1 Damage

The first category is damages or defects which will remain undetected. The component must retain the capability to support the ultimate loads for the entire component life [9]. This includes undetected manufacturing defect and Barely Visible Impact Damage (BVID). Category 1 damages will never be repaired. BVID is the main focus of this research.

Category 2 Damage

When damage is reliably detected during scheduled inspections it falls under category 2 damage. This can be called Visible Impact Damage (VID) and Clearly Visible Impact Damage (CVID). Because this type of damage will be repaired during maintenance it is allowed that the residual strength is reduced. The required residual strength depends, among other factors, on the probability of occurrence and the inspection interval.

Category 3 Damage

If damage will be reliably detected by the flight crew within a few flights it falls under category 3 damage. It is required that this type of damage can be detected by someone with no knowledge of aircraft maintenance or damage in composites. The required residual strength of the component is reduced to the limit loads and will be repaired immediately after detection.

Category 4 Damage
Impact damage that is caused by an impact event that is noticed by the flight crew when it takes place is called category 4 damage. This means the pilot is aware that the aircraft is damaged and can take action to lower the structural loads on the aircraft. The pilot must land the aircraft directly after the impact event and the aircraft has to be repaired directly after this flight.

Category 5 Damage
Category 5 damage is damage that happens as an anomaly. This means it is not taken into account during design or manufacturing. It still is listed in AMC 20-29 [9] to emphasise the importance of reporting anomalies during aircraft operations. Examples are very hard landings or collisions with ground equipment. Even though the aircraft may look fine after these anomalies it is extremely important to take appropriate action because the surface may hide severe structural damage.

2.2.2. Detectability
As mentioned in subsection 2.2.1, impact damage is categorized based on detectability for certification. The detectability in this case means the ease at which impact damage can be detected. Impact damage can be detected at two different inspections. At the preflight inspection before every flight or at the maintenance inspection at every maintenance interval. Damage that is detected during preflight inspection is also called obvious damage. The smallest damage size that will be reliably detected during maintenance inspection is set by the detectability threshold.

Detectability Threshold
Scheduled maintenance will be performed once every maintenance interval. During maintenance a detailed inspection is performed of the aircraft. The lower limit of the damage size that is reliably detected during this inspection sets the border between category 1 and 2 damage. In the Composite Materials Handbook, volume 3 chapter 12 [1] this border is called the detectability threshold. In this handbook it is recommended to perform a Probability of Detection (PoD) study to find this detectability threshold. Indentation is often used as a measurement to characterize the damage size and was also used to set the threshold. The detectability threshold can also be referred to as the BVID size.

The BVID size represents the size of damage that corresponds to a Probability of Detection (PoD) of 90% at a 95% confidence level [1]. In simpler terms, if we were to plot the depths of indentations for damages with a 90% PoD on a graph, the BVID is the upper boundary of the interval which will capture 95% of the damages. It's important to note that the PoD is influenced by various factors such as the depth of indentation, damage diameter, type of inspection, inspection distance, the qualifications of the inspector, and the color of the substrate.

In the Composites Materials Handbook [1], the detectability threshold is assumed to be between 0.25mm and 0.60mm after relaxation. It is clear that this value varies greatly in literature. In Table 2.1 the values used by other companies are shown. The original sources of the publication of these values are hard to find. It is however clear that these values vary greatly. It is however noteworthy that the largest values in this table are from the US Air Force and the US Navy. The original source was not found and the reference trail leads to Rouchon [10] who mentions that these are values used for military applications and not civil aviation. The trail ends at Kan. et al. [11] who mention the values but discard them. There is an ISO standard, ISO 18352:2009(en) [12], that sets the BVID size at 0.30mm. It is clear from this that this value is highly dependent on the circumstances which means a PoD study will have to be performed when determining the detectability threshold for a certain part. This can be based on literature or on physical tests.

Table 2.1: Comparison of Different BVID Values Found in Literature. [13–16]

Company	Aerospatiale	Boeing	Airbus	USAF	US NAvy	CAA
BVID size, mm	0.3	0.25	0.3	2.5	1.25	0.25

2.2.3. Current Practice

The current industry standard for demonstrating the impact damage tolerance of composite structural components usually consists of a combination of testing, analysis, and simulation. Companies typically form a certification strategy that includes design requirements, testing standards, and certification guidelines set by regulatory agencies, such as EASA's AMC-20-29 [9] document. This approach follows a "Safety by inspection" methodology, allowing damage to remain as long as it can be identified and repaired, or if the damage poses no threat to the aircraft's structural integrity [17].

Testing encompasses the execution of impact tests on both specimens and full-scale components, aimed at assessing the magnitude of damage inflicted and the remaining structural strength of the component. Analytical and simulation methods, such as finite element analysis (FEA), come into play to predict the component's reaction to diverse loading scenarios [18]. Frequently, compression after impact (CAI) tests are employed to establish a maximum permissible strain. This strain value represents a reduction from the actual structural performance to accommodate any potential impact events.

Non-destructive evaluation (NDE) techniques such as ultrasonic inspection and thermography are also used by companies to detect and monitor damage in real-time. The certification process usually involves a comprehensive documentation package that includes testing reports, analysis results, and NDE inspection records. This process is often allowed to take place while the aircraft is already in service [11].

The certification strategy used by PAL-V is taken from the Composites Materials Handbook [1]. Fatigue testing will be performed on the structural components in which certain impact damages will applied at various intervals. The test starts with category 1 damages already present as this type of damage can exist in the part for the entire lifetime. After one entire lifetime is simulated category 2 and 3 damages are applied after which the part is fatigue tested again for the expected interval after which this damage is expected to be detected and repaired. An example of this fatigue test sequence is shown in Figure 2.2. At certain moments during the fatigue test the limit load or ultimate load is also tested. At the end of the entire fatigue test the failure load will also be determined. To successfully execute this test it is required to accurately apply the exact amount of impact damage to the component.

This accurate application of impact damage is challenging. The exact energy that is required to inflict a certain impact damage is unknown and dependent on many factors. Currently a lot of impact testing is done to determine the impact energy for certain damage categories. When one impact test is performed the component can be structurally compromised. This may require a new component for every single impact test.

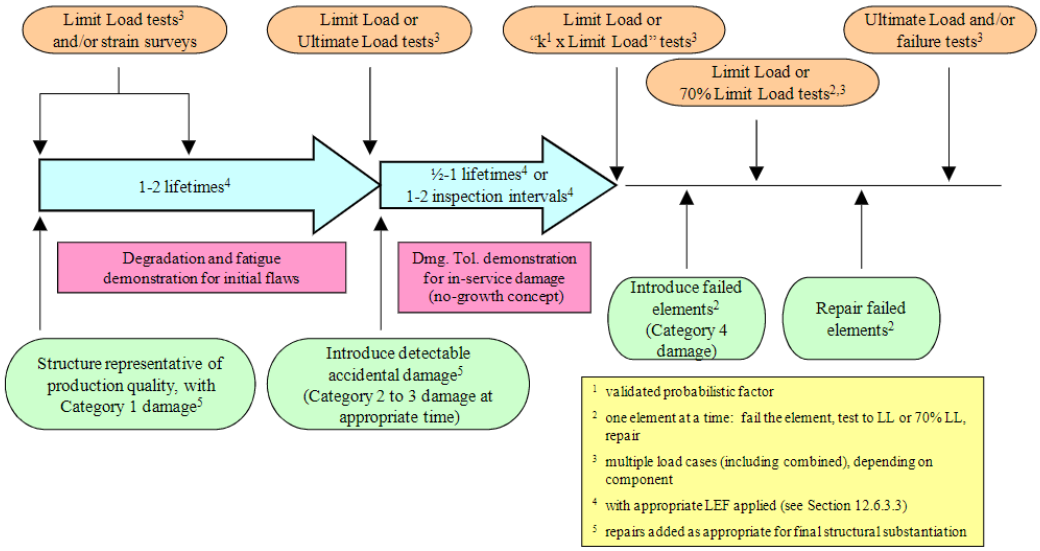

Figure 2.2: Fatigue Test Sequence Example. [1]

2.3. Impact Damage Mechanics

In this section the structural mechanics at play during an impact event are explored. These structural mechanics were used to determine what parameters influence the impact damage event and what models can be made to approximate this.

2.3.1. Impact Structural Response

The structural response of a component during an impact event will change the velocity of the impactor. This response is a combination of elastic effect and damage effects. The contact force history, which is the force between the impactor and the target over time, can characterize an impact event [19]. A good indicator of the intensity of an impact event is the kinetic energy of the impactor.

Elastic Response

The elastic response of the target is the ability of the target to deform temporarily. In the most basic sense this can be approximated by a mass hitting a spring with a velocity. The spring will apply a contact force to the mass which will eventually release the mass with the same velocity in the opposite direction [20]. In practice this would mean that when an impactor hits a target, the target will deform elastically and the impactor would bounce without leaving any damage on the target. Another analogy is that the kinetic energy of the impactor is stored as spring energy in the target. This spring energy is then reapplied to the impactor which restores the kinetic energy in the opposite direction. This is only possible if the internal loads in the structure never exceed any material strengths.

How the target reacts elastically will depend on the properties of the target like the stiffness and boundary conditions. However it is also determined by the impact velocity and in term the impact duration. This is further explained in subsection 2.3.3. A carbon fiber structure will have a stiffer elastic response when undergoing impact loading compared to quasi-static loading [21]. This is due to the composite structure getting stiffer at higher loading rates.

Damage Response

When the internal forces inside the target exceed the ultimate material strength, the target is damaged [22]. This damage changes the contact force history and therefore the velocity of the impactor. When a section of a structure fails, the energy stored as spring energy is dissipated and not returned to the impactor. The overall stiffness of the structure will be reduced which also changes the elastic response of the target [23]. The damage modes are further discussed in subsection 2.3.2.

Indentation

After an impact damage event, a permanent deformation of the surface, or a dent, can be visible. This dent is referred to as the indentation. This is often an indicator for the amount of visible damage left behind. The indentation is created by local fiber failure, or core crushing [24]. Indentation in sandwich structures can be enhanced by the relatively weak core which can prevent the skin from returning to the initial position [25].

Relaxation

The indentation left behind after an impact damage event is known to reduce in depth over time. This is called relaxation [16]. This relaxation can reduce the indentation up to 3 times but usually the residual dent depth is 70-80% of the initial dent depth [26]. Dubinskii et al. [14] have shown that this relaxation can take up to 200 days to reach equilibrium and is heavily influenced by temperature and moisture. Relaxation usually follows a logarithmic approximation as shown in Figure 2.3.

2.3.2. Damage Modes

Within the field of composite engineering, various modes of damage can occur when a component is subjected to an impact event. It's important to distinguish between failure modes occurring within the skin or monolithic structure and those specific to sandwich structures.

Skin Damage Modes

In this section the damage modes in the skin resulting from an impact event in composites will be explored. These damage modes can occur in both the skin of sandwich structures as in monolithic parts. These damage modes are shown in Figure 2.4.

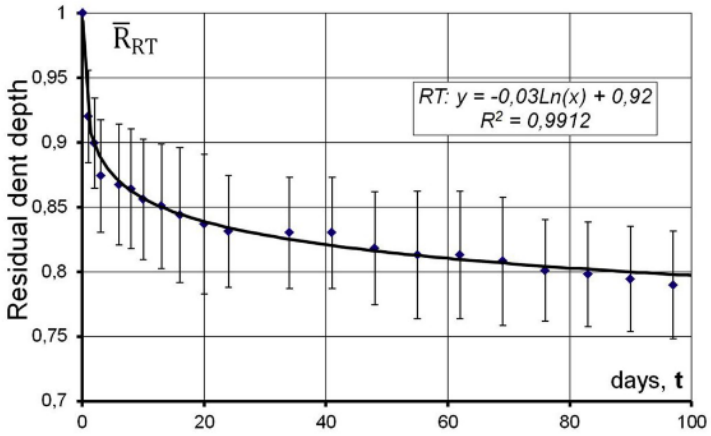

Figure 2.3: A Typical Relaxation Graph of Dent Depth in Carbon Composites [14]

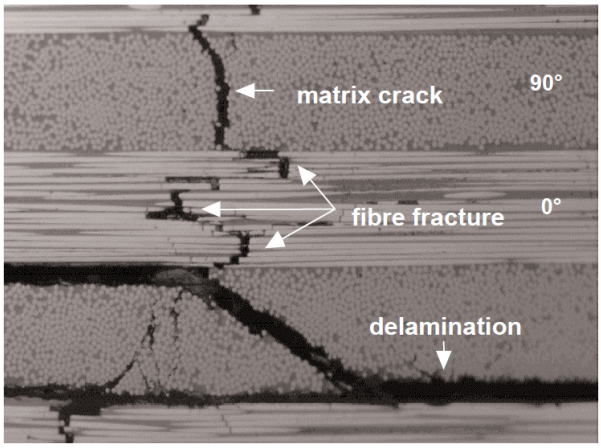

Figure 2.4: Damage Modes in Composites. [27]

Delamination

Delamination is the separation of two adjacent fiber layers inside a laminate. In Figure 2.4, delaminations are visible as the horizontal black lines inbetween the fiber layers. The main factor causing delaminations is the mismatch in directional stiffness between the fiber layers due to a fiber direction change between adjacent layers [19]. This failure mode is matrix dominated because there are usually no fibers passing between the fiber layers.

Matrix Cracks

Matrix cracks are, just like delaminations, matrix dominated failure modes. Matrix cracks are also shown in Figure 2.4. The main difference is the fact that matrix cracks are cracks that pass through a fiber layer. This is only possible if the crack is oriented along the fiber direction, otherwise this would mean that fibers have to be broken. Matrix cracks often occur when the bond between the matrix and a fiber is broken [19].

Fiber Fracture

Fiber fracture can be divided into local and global fiber fracture. Local fiber fracture will happen at the interface between the impactor and the structure and is the main cause of permanent indentation [28]. Global fiber fracture happens at much higher internal stresses than matrix dominated failure modes. This is because of the high material strength of the fibers compared to the polymer matrix. This damage mode, just like matrix cracks, forms cracks in between the fiber layers [19]. These cracks are oriented perpendicular to the fiber direction as shown in Figure 2.4.

Sandwich Damage Modes

Sandwich structures can exhibit additional damage modes following an impact event that are not observed in monolithic structures. These specific damage modes are shown in Figure 2.5.

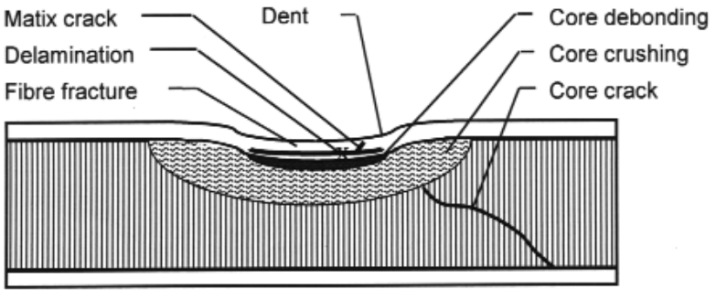

Figure 2.5: Damage Features in Composite Sandwiches. [27]

Core Crushing

When the skin deflects into the core, the core is also compressed. When the core fails it is unable to restore the original shape after the compressed sandwich is released [29]. Usually a sandwich core is made to be lightweight. This means there are a lot of air pockets inside the core like the bubbles in foams or the holes in a honeycomb core. This weakens the core in compression [27].

Core Cracking

The core will crack if it fails in shear or in tension. This means the core can no longer transfer loads through this cracked plane [27]. This happens when the internal shear or tensile loads in the core exceed the ultimate material strength of the core.

Debonding

Debonding refers to the separation of a sandwich structure's skin and core. This typically occurs when the core is crushed, allowing the skin to rebound more extensively to its original position compared to the core. In cases of skin and core debonding, the flex back of the skin can conceal any underlying damage to the core [27, 29].

2.3.3. Velocity Regimes

Impact events with the same energy have similar results when the impact velocity, or the impact time, is in a similar velocity regime [5, 19, 30]. These regimes are largely determined by the deflection rate compared to the speed of sound in the material [1]. This means that impact events which have equal impact energy can still result in a different response.

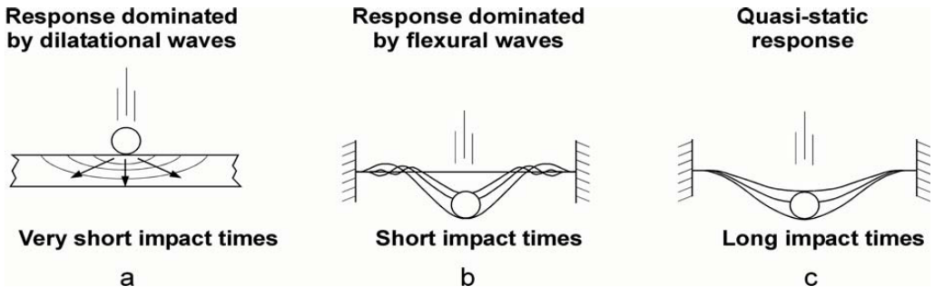

Figure 2.6: Response Types or Velocity Regimes for Impacted Structures.[27]

Low Velocity Impact

At low velocities, impact events are considered quasi-static [19, 27]. The speed at which the impact load is applied is not relevant. This means that the internal load transfer or wave propagation has to be significantly faster than the change in deflection. In this velocity regime the boundary conditions and overall structural properties of the impacted structure are driving the deflection response of the plate. This regime is shown in Figure 2.6(c). Low velocity impacts examples are tool drops or a collision with ground equipment.

Intermediate Velocity Impact

At intermediate velocities, the flexural waves and shear waves inside the structure become relevant. The problem can no longer be considered quasi-static. The change in deflection by the impactor is fast enough to excite certain wave modes in the structure [27]. This is shown in Figure 2.6(b). This means the boundary conditions are still relevant, but don't dominate the structural response. Here the mass of the plate also becomes relevant.

High Velocity Impact

In high velocity impacts, the impact event is over before flexural and shear waves through the structure are created [19]. The impact response is dominated by the local three-dimensional wave propagation [27]. The boundary conditions of the structure are not relevant anymore. The local mass of the structure together with the mass of the impactor largely determine the deflection response.

Hyper Velocity Impact

Hyper Velocity is in the regime of multiple kilometers per second. In this case the solid behaves like a fluid [19]. This velocity range is not encountered in regular aviation or road use. It will not be discussed further in this report.

Damage Associated with Velocity Regimes

The damage done by an impactor is different for the different velocity regimes even if the impact energy is the same. High impact velocities tipically cause more damage to the target than low impact velocities [19][31][27]. This is caused by the high velocity and low impact time causing a stiffer response, due to the wave velocity, and a higher peak force [27]. However, even though high velocity impact causes the most damage, this is not considered the damage regime which is the most dangerous in aeronautics.

The most dangerous impact events in aviation are the events that cause the most amount of damage without leaving a visible indication. This will be further explained in section 2.2. Van Hoorn et al. [32] have shown that a low velocity impact event causes more internal delamination compared to a high velocity impact event at the same indentation depth. Low velocity impact can also cause more damage to the sandwich core than high velocity impact for the same dent depth [33].

The Velocity Regime Ranges

As mentioned in the introduction of subsection 2.3.3, the velocity regimes are used to be able to compare different impact energy levels. It is important to set the range of the velocity regimes such that this comparison is not assumed to be accurate while in practice this will not be the same.

While it is commonly accepted that low velocity impact is considerably different to high velocity impact, a clear border between the regimes is not common. Often a certain velocity is used to indicate the border between two regimes. The maximum velocity for an impact event to be considered low velocity is often set around 10-20 m/s [5, 19, 30, 32]. The impact event is considered high velocity impact when the velocity is higher than 11 m/s [30], 70 m/s [27] or 100 m/s [19, 32]. It is clear that below 10 m/s can be considered low velocity and above 100 m/s high velocity. Based on preliminary assessment we will be expecting impact velocities between 0-50 m/s which can be considered low to intermediate velocity impacts. However, in Figure 2.3.3 it is stated that low velocity impact is the most dangerous type of impact for composite structures in aviation.

2.3.4. The Effect of Prestress Conditions

Robb et al. [34] have shown that tensile prestress does increase both the damage area as the indentation depth but have also concluded that no significant difference can be found for strain levels below 2000 $\mu\epsilon$. Whittingham et al. [35] analysed impacts during 1000 $\mu\epsilon$ and 1500 $\mu\epsilon$ tensile pre-stress

and have concluded that at these strain the pre-stress has not significantly affected the peak force, absorbed energy and indentation depth. Zheng and Binienda [36] have shown that pre-stress does influence the displacement at the impact location. Guillaud et al. [37] have shown that the pre-stress increases the contact force and the sum of the delamination area while decreasing the damage area and impactor displacement. The sum of the delamination area and contact force are not significantly changed below 1500 $\mu\epsilon$.

Hu et al. [38] have determined that a tensile prestress actually increases the residual tensile strength and bending modulus. Panciroli et al. [39] have concluded that tensile prestress increases the induced damage and contact force while decreasing deflection but have only compared samples with zero prestress to samples with 6000 $\mu\epsilon$.

2.4. Determining Impact Energy Level for BVID

As highlighted in section 2.2, it becomes evident that ensuring precise application of impact damage to the propeller is essential when conducting fatigue testing for certification. This process begins with the determination of the necessary impact energy to inflict (BVID) in the propeller.

2.4.1. Models

One way to determine the impact damage response is by using analytical or numerical models. When using models, physical testing can be partially replaced by calculations.

Analytical Models

A complete model is a model that combines the dynamics of the structure, projectile and contact behaviour. This model uses classical plate theory to determine the plate dynamics [19]. The projectile is usually modelled as a rigid body and the contact behaviour by an appropriate contact law. This results in a highly complex model with many non-linear relations [19]. This will in turn result in a problem which requires a lot of computational power to resolve. Esrail and Kassapoglou [40] have made an efficient approach to solve a complete model but it still takes between 5 and 10 minutes for a coupon sized component. When expanding the equations to a complex part it can quickly become a lot longer and less accurate. It would be better if the problem could be simplified.

Shivakumar et al. [41] have created a two degree-of-freedom spring mass model which is an extension to a spring mass model created by Lee [42]. This model consists of two masses connected with springs. One mass represents the projectile while the other represents the target. The contact behaviour between the two is modelled as a spring and the boundary conditions modelled as multiple springs. A schematic of the model is shown in Figure 2.7. This model is useful for analysing boundary controlled, or low velocity, impact. In this model the mass of the impactor and the plate are represented by M and M_p respectively. The contact stiffness, boundary stiffness, shear stiffness and membrane stiffness are represented by k_α, k_b, k_s and k_m respectively [27].

When the impact velocity is high enough to be considered wave controlled impact, the boundary conditions are no longer relevant. A different model can be used in which the response of the target is represented by a spring and damper. This model is shown in Figure 2.8. The damper is used to approximate the response of the plate. This response is entirely dependent on the local plate properties and not on the boundary conditions [27, 43].

Numerical Models

Numerical models can be used to simulate an impact event. A wide variety of literature is available which describes a finite element method and compares this method to experimental results [33, 44, 45]. The difference between the models often is the way the damage is predicted. These models often are able to predict the damage quite accurately but are limited when predicting permanent indentation [44, 45]. Unfortunately finite element models often require expensive software and computational resources. These models simulate impact damage on a flat coupon of 150x100mm. Expanding this simulation to larger, more complex geometries will greatly increase the model complexity, cost and possible inaccuracies.

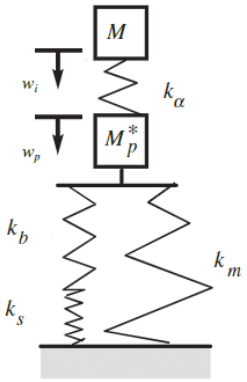

Figure 2.7: A Spring and Mass Model for Boundary Controlled Impact. [27]

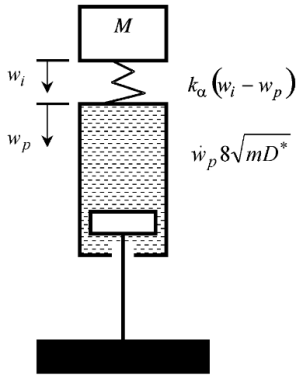

Figure 2.8: A Spring, Mass and Damper system for Wave Controlled Impact. [43]

2.4.2. Physical Testing

Another way to determine what indentation will result from an impact event is by physical tests. Low velocity impact testing is usually done via drop tower [1, 19]. In the testing standard ASTM D7136 [46] the setup for performing these drop-weight impact tests is explained. The test consists of a guided mass being dropped on a composite target. The energy is varied by changing the drop height or by changing the mass of the drop-weight. The speed of the impactor is measured just before the impact event to determine the actual impact energy. The drop-weight has a hemispherical tip pointing down towards the target. This tip can be varied but is set at a radius of 16mm for the ASTM D7136 standard. In this standard the target is a 100x150mm flat coupon and is used to determine the impact resistance of the material or to prepare the material for compression after impact testing [46]. The test setup used in the ASTM D7136 standard is also widely used to perform drop-weight impact testing on different targets [32, 33, 47]. This test has to be repeated until enough data is gathered to determine the impact damage resistance of the material and layup.

These flat composite coupons can be representative of a large stringer reinforced component like a fuselage section. However when the size of the part approaches the size of the flat coupon this can no longer be assumed [48]. In the case of a composite propeller, both the shape of the specimen as well as the in use boundary conditions differ from the flat plate samples commonly used in drop-weight testing.

It is clear that the boundary conditions have a large influence on the damage inflicted by a similar impact event [49–51]. In subsection 2.3.3 it is already stated that a stiffer response causes a larger indentation and can reduce internal damage at the same impact energy level. From AMC 2029 [9] it is clear that the fatigue evaluation has to be performed with BVID in the most critical case. This is both the most critical location on the component and the most severe internal damage possible caused by the BVID inducing impact event. This means it is important that the way the component is fixed during the application of the BVID to the propeller does not reduce the internal damage created compared to the real in-service case.

From this it can be concluded that the impact tests need to be performed on a complete propeller blade with the proper supports. The fact that a lot of tests need to be performed to determine the impact damage response also means that a lot of propeller blades have to be used in this process.

2.4.3. Quasi-Static Loading

As mentioned in subsection 2.3.3, low velocity impact is often referred to as quasi-static loading which means the loading can be considered static. This means that the rate at which the deflection is created by the impactor has no effect on the results [19, 30, 52]. In physical testing one could assume that this means a low velocity impact event simulated by a drop-weight impact test can be interchanged by a compression test bench applying a load with similar peak force and deflection. This has been investigated in the past. Some studies have found that this is the case [53–55] other studies found that there is a difference [56, 57].

Highsmith [56] calculated the equivalent impact energy from a quasi-static load curve by integration. The peak force found at this impact level was 5-10% higher than during quasi-static loading. He also found that the damage area during quasi-static loading was larger than during impact loading. Breen et al. [57], who did a FE analysis, also found that when the impact velocity increases, the damaged area decreases. Breen et al. [57] only went as low as 2 m/s impact velocity and calculated the impact force by the acceleration and mass of the impactor. This makes it hard to compare it to loading rates that are lower. The first few impact velocities also show large differences in impactor force between very similar impact velocities which could also indicate low accuracy in the model or force calculation at low impact velocities. Unfortunately these studies did not analyse the dent depth.

Belingardi and Vadori [55] concluded that there is no difference between quasi-static and impact loading when looking at impact force. The dent depth was not analysed. Lawrence and Emerson [58] found that although both the dent depth and internal damage differ between low velocity impact and quasi-static loading, the compression after impact strength is similar. Spronk et al. [59] have shown that, for carbon epoxy laminates, the maximum force and dissipated energy are the same while the dent depth is overestimated when using quasi-static loading.

From these studies it seems like the peak impact force can be estimated using quasi-static loading but the dent depth and damage area is not similar. The studies agree on most aspects here but draw the conclusion from different aspects. Peak force and dent dent seem to be correlated [60, 61]. When this correlation is known, quasi-static loading could be used to predict an impact energy level which will create a certain peak load and through this correlation a certain dent depth.

Impact testing can only be done at one energy level at a time. Setting the correlating impact energy during quasi-static loading is done by stopping the displacement. This means that if the displacement is continued, the reaction of the target can be mapped during one test with only one coupon or component.

2.5. Literature Conclusion

It is clear that impact damage poses a significant threat to carbon composite structures. Low velocity impact events pose a threat in particular because these impact events create the most severe internal damage when leaving a barely visible dent. For certification it is necessary to inflict BVID to the propeller before fatigue testing which requires a way of predicting the energy required to create BVID. The most feasible way of doing this is by doing physical impact tests. Coupon testing alone is not sufficient for the complex and rather small geometry of the propeller and only doing impact tests on complete composite propellers will mean that a large quantity of propellers are needed to determine the impact damage characteristics.

Creating a link between low velocity impact testing and quasi-static loading can mean that the local impact damage response is determined on simple and cheap coupons while the overall structural response of the part is mapped during quasi-static loading. This would mean that only a few propellers are needed for determining and validating the propeller impact damage response and especially for predicting at what impact level BVID is inflicted.

2.6. Research Questions

The goal of this research is to develop a method to inflict BVID to a carbon composite propeller blade which can be used for certification while minimizing the resources required. After the literature review a gap in the knowledge was found which could lead to such a method. The research question for this research will be:

How can ASTM D7136 impact testing and quasi-static loading be used to predict the impact energy required to induce Barely Visible Impact Damage (BVID) for the certification of carbon composite propellers?

This question is further divided into sub-questions. Only when these sub-questions are answered can the main research question be addressed.

1. What are the requirements for impact damage to be considered BVID on the propeller for certification?
    (a) What are the impact threats for the propeller?
    (b) Where on the propeller should the impact damage be applied for certification?
    (c) What can be considered Barely Visible Impact Damage (BVID) on the propeller blade?
2. How do the results of ASTM D7136 testing correlate with the mechanical response of a similar coupon under quasi-static loading conditions?
3. How does the mechanical response of a coupon under quasi-static loading conditions correlate with the mechanical response of a propeller blade under similar loading conditions?
    (a) What are the boundary conditions on the propeller when the BVID is expected?
    (b) How can a clamping mechanism mimic these boundary conditions on the propeller during testing?
4. How can a prediction be made of the impact response of the propeller using coupon testing and propeller quasi-static testing?

3

Methodology

During this research a new method of impact damage prediction was tested on the propeller blade of the PAL-V Liberty. The new method consists of doing a threat assessment with a Probability of Detection (PoD) study, performing ASTM D7136 impact testing, performing quasi-static testing on coupons, performing quasi-static testing on the propeller blade and performing impact testing on the propeller blade. The hypothesis was that the Low Velocity Impact (LVI) damage response of a carbon composite propeller can be predicted by a model using results from coupon impact testing and quasi-static testing.

It is known that there is a difference between impact and quasi-static loading. In the method proposed here this difference was explored and documented for a certain type of material on coupon level. This known difference was then used to link the quasi-static behaviour of a larger component, like the propeller blade, to the impact behaviour of this component. The plan was that one impact test usually ruins the specimen. If all of these impact tests were performed on the propeller blade each test would be very expensive. The structural response during quasi-static loading can be explored in only a few tests even without breaking the component. This meant that if the quasi-static response could be linked to the impact response accurately, very few propeller blades would be needed in the end to map the propeller impact response.

The threat assessment determined the impact location on the propeller which was considered the most critical. This location was also the location on which all the other tests and the model were based. The threat assessment also determined what the impact energy range was that had to be considered for certification.

The PoD study sets the limits of the BVID range. This determined what the size of the impact damage was for this damage to be detected during inspection.

ASTM D7136 coupon impact testing analysed the impact event that creates BVID. The impact energy, resulting dent depth and contact force were used to determine the characteristics of the impact event.

Quasi-static testing was performed on coupons to determine the difference between impact loading and quasi-static loading. This information was used to determine the response of the propeller from quasi-static propeller tests. Propeller quasi-static testing was performed to map the structural characteristics of the propeller. This information was used along with the knowledge gained from ASTM D7136 impact testing and quasi-static coupon testing to create a model. Using this model it was attempted to predict the outcome of the final tests.

The final tests performed were impact tests on the propeller blade. These tests served as validation of the model and determined the success of impact damage prediction using this proposed method.

4

Threat Assessment

In this chapter a threat assessment was performed to explore what impact threats exist which are a risk to the structural performance of the propeller. The goal of this chapter was to determine a location on the propeller blade at which BVID will be applied for certification. It was also determined what the impact parameters are of the impact threats.

First, in section 4.1, it is stated what a threat assessment is and why it is performed. Section 4.2 will provide the characteristics of the PAL-V Liberty propeller. In section 4.3 the location was determined at which the structural consequence of an impact damage event will be highest and in section 4.4 the impact sources are identified. Finally, in section 4.5, an impact energy range is determined after which the conclusions are drawn in section 4.6.

4.1. What is a Threat Assessment?

A threat assessment in this case will be performed to identify what objects will be able to hit the propeller and cause damage. In ”Risk Assessment: Theory, Methods, and Applications” by Rausand [62], this form of threat assessment is called a risk analysis and has three steps:

1. Hazard identification
2. Frequency analysis
3. Consequence analysis

The hazard identification aims to identify any threats related to the system. In this case the threats are objects which can create impact damage on the propeller. The frequency analysis will identify the probability of the impact events. According to the Composite Materials Handbook [1] this can be used to determine a cut-off energy level at which the impact event can be assumed too rare to be considered. The consequence analysis will determine what consequences the impact events have. In this case the amount of structural damage resulting from a specific impact event is the relevant consequence. The consequence of the failure of the propeller is already known and taken into account in the overall vehicle design. That is why this section will focus on the location of the impact damage on the propeller blade and more specifically at which location BVID will have the most severe structural consequences.

Of these three threat assessment steps, the consequence analysis is in this case done first. This is to select a critical location on which the other sections can focus. To do this, first the propeller characteristics are explored. After that the hazards are identified. The last section will explore the frequency analysis to determine an energy cut-off.

4.2. Propeller Characteristics

In this section the characteristics of the propeller are explained. This helped in determining the most critical impact location.

4.2.1. Propeller Cross-section

The cross-section of the propeller is shown in Figure 4.1 The thicker sections in this cross-section are called the spar and the thinner sections are called the skin. On the inside of the skin and spar is a foam core. In this cross-section, four impact options are shown. Number 1 indicates an impact with an impactor directly onto the leading edge of the propeller. Number 2 and 4 indicate an impact on the spar near the middle of the propeller blade. Number 3 indicates an impact on the skin near the middle of the propeller blade. The side at which number 2 and 3 are pointing will be referred to as the back of the blade. The side at which number 4 is pointing will be referred to as the front of the blade.

An impact on the leading edge, number 1 in Figure 4.1, would result in a very stiff response. The spar on both sides of the leading edge will support the load in plane. Thorsson et al. [63] have shown that edge on impacts lead to BVID with less structural damage compared to face-on impacts. It is clear that an impact here will probably lead to visible damage without damaging the structure of the propeller.

An impact on the spar, number 2 or 4 in Figure 4.1, would result in a more flexible response compared to number 1. This means that the spar will flex more and this will lead to a higher risk of internal damage. This impact location is also close to a ply drop. A ply drop can increase the structural damage done by a certain impact event as it functions as a crack initiation site for delaminations [64].

An impact on the skin, number 3 in Figure 4.1, will have a low impact on the structural integrity of the propeller. The skin is not designed to support large structural loads and if this section is damaged, it would not lead to a significant loss in overall structural properties.

When only looking at the propeller cross section it was concluded that an impact on location 2 or 4 was expected to inflict the most structural damage inside the propeller. This information was used to determine the overall critical location on the propeller blade.

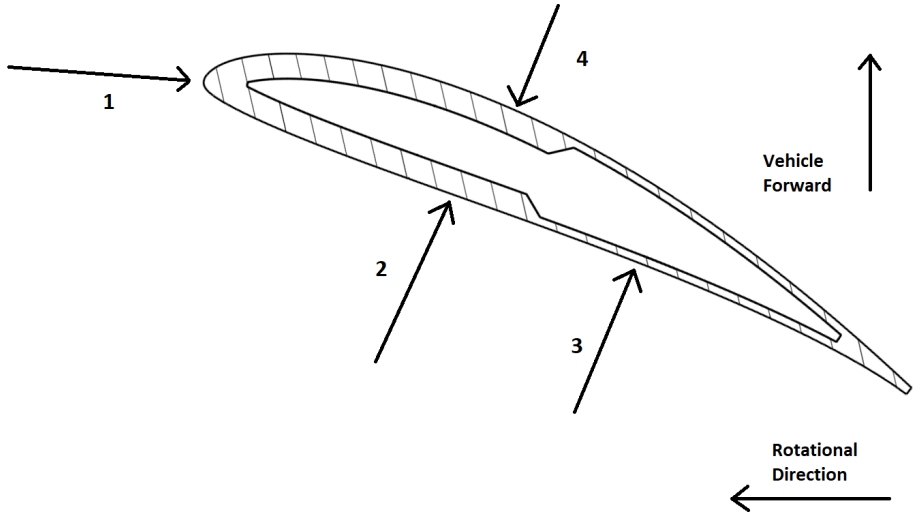

Figure 4.1: A Cross-section of a Carbon Fiber Propeller.

4.2.2. Propeller Velocity

When the PAL-V Liberty is being used in fly mode, the propeller will be spinning. This will make the impact velocity on the propeller blade dependent on the radius at which an impact event could occur. At the maximum design RPM the propeller is spinning at 2600 RPM or 273 rad/s. The propeller local velocity is plotted against the radius during this maximum RPM in Figure 4.2. The maximum velocity is found at the tip at 259 m/s.

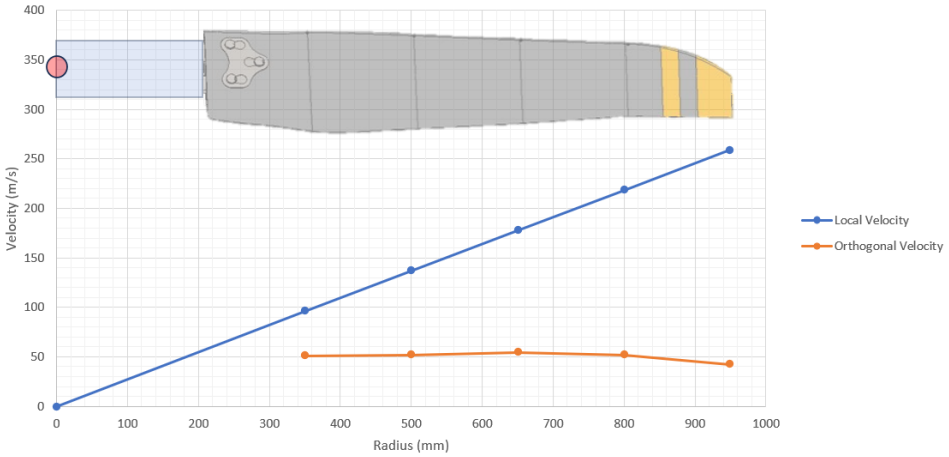

Figure 4.2: The Propeller Velocity and Orthogonal Velocity as a function of Radius.

4.2.3. Propeller Geometry

In Figure 4.3 it is shown that the angle of the propeller blade various throughout the radius. The exact angles are confidential but the angles vary between 55 and 80 degrees. This has to be taken into account when the angle at which an impactor can hit the propeller is determined. The highest impact velocities are achieved for two different cases for the front, number 4, and back, number 2, of the propeller.

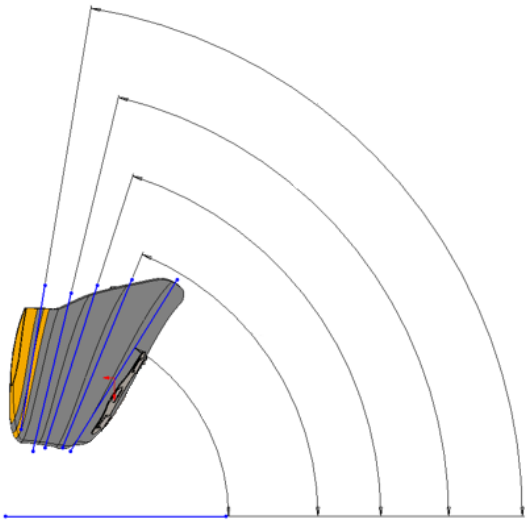

Figure 4.3: The Variation in Blade Angle of the Propeller.

For an impact at number 4 in Figure 4.1, the worst case will be when the propeller is stationary and the vehicle is moving at the highest speed. This would be when landing with an engine out. The maximum velocity of the vehicle and the impact will be 30 m/s. In practice the propeller will be spinning at this vehicle velocity due to the incoming air. This will reduce the perpendicular impact velocity. Impact location number 4 will also have an angle compared to the vehicle forward direction reducing the impact velocity even more.

The worst case for an impact at number 2 in Figure 4.1 will be when the propeller is spinning at maximum RPM while the vehicle is stationary. This means the velocity in the rotational direction is highest while the vehicle forward direction is 0. In Figure 4.2, the orthogonal velocity of an impactor hitting the spar of the propeller, number 2 in Figure 4.1, is plotted as well. This velocity is fairly constant at 50 m/s for the entire propeller due to the twist in the propeller blade.

4.3. Consequence Analysis

This consequence analysis explored what impact event will have the most severe structural consequence at BVID level. A possible critical impact location was selected based on the internal loads. This location was verified further on in this chapter. The location identified in this section influences the possible impact hazards.

4.3.1. Propeller Internal Loads

During the design of the propeller, the internal strains were analysed. The internal strain in the propeller skin and spar are plotted in Figure 4.4 and Figure 4.5 respectively. For both cases the propeller was loaded with a maximum RPM load case with the associated aerodynamic forces and moments. The exact strain values are removed from the plots for confidentiality.

From these illustrations it is clear that the propeller is most critical at the back of the blade. The area near the root shows more strain than the area near the tip. In Figure 4.5 a strain concentration is visible at the blue circle.

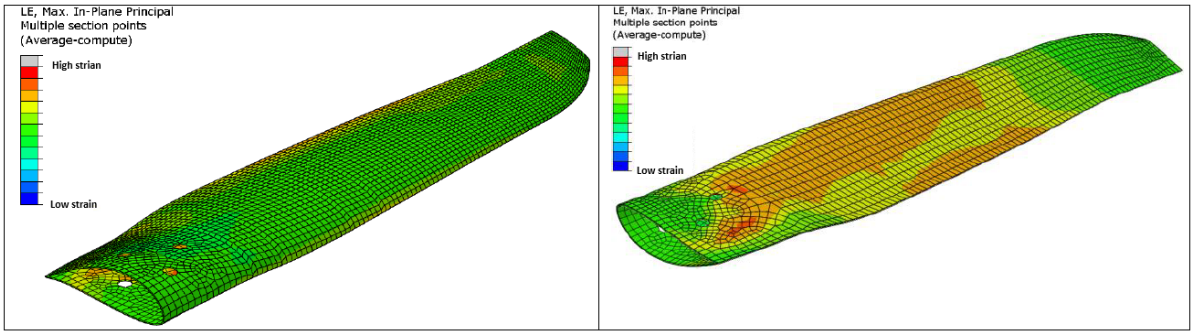

Figure 4.4: The Strain in the Skin of the Propeller in Microstrain. image credit: PAL-V

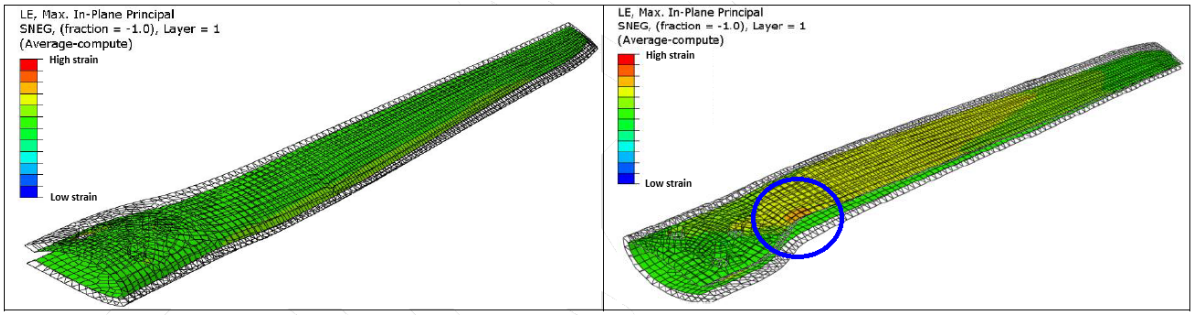

Figure 4.5: The Strain in the Spar of the Propeller in Microstrain. image credit: PAL-V

4.3.2. Critical Impact Location

From subsection 4.3.1 a possible critical impact location was selected. The location indicated with the blue circle in Figure 4.5 was considered the most critical. This location corresponds with location 2 in subsection 4.2.1 and subsection 4.2.3 which also identified location 2 as a critical impact loaction on the propeller cross-section. It is located at 260 mm from the root of the composite propeller blade on the back side of the blade. It is located on the spar just before the transition into skin. It has an angle of 62° relative to the vehicle forward direction when mounted on the vehicle.

This location was selected for the main reason that there exists a concentration of strain at this point. But for this location to be considered the most critical the impact threat also has to be high. If this is the case was analysed in section 4.4.

4.3.3. Prestress in the Impact Location

The internal strains in the propeller blade while spinning at maximum RPM is shown in Figure 4.4 for the skin and Figure 4.5 for the spar. The scale in these figures is removed but in the critical location, the internal strain is between 750 and 1000 $\mu\epsilon$ or micro strain. This can alter the impact response of the material. What the influence is of tensile prestress on a low velocity impact event was analysed in subsection 2.3.4. In this section it was determined that if the strain is below 1500 $\mu\epsilon$ there is no significant effect on the impact mechanics.

From this it was concluded that although the prestress does have a significant effect on low velocity impact damage, it does not have a significant effect at the strain levels inside the propeller blade spinning at maximum RPM. It is expected that the deflection will be affected but the contact force, indentation depth and internal damage will not be changed between the stationary and rotating propeller blade.

4.4. Hazard Identification

This section aims to identify the hazards which in this case are the possible projectiles which can hit the propeller. There are many potential sources of projectiles. They can generally be categorized in the following [28]:

- Tool Drop
- Runway Debris (Foreign Object Debris)
- Bird Strike
- Hail
- Foot Traffic or Luggage
- Ground Service Equipment

One situation that is new for PAL-V compared to other aircraft is driving on the road. This means it was necessary to explore the risks of an impact event on the propeller during road use.

4.4.1. Tool Drop

There are two scenarios in which the propeller can be struck by a tool. When the propeller is on the aircraft or when the propeller is not on the aircraft. When the propeller is on the aircraft the highest a tool can drop is when the aircraft is in flight configuration and work is being done on the rotor. In the case of the PAL-V Liberty the distance between the extended propeller and the rotor system is 1.91 meter. This is shown in Figure 4.12. When the propeller is not on the aircraft the propeller can be on a bench. In this case the potential drop height will be much lower. The propeller can also be on the ground in which case the drop height can be similar to the 1.91 meter mentioned before.

Typical tools used could be wrenches for bolts or hammers for pins. A typical hammer does not weigh more than 1 kg. A small Allen wrench does not weigh more than 50 grams but a large wrench could weigh as much as 1.8 kg if you include torque wrenches. When impact wrenches are used, it could be as high as 3 kg. When the propeller is mounted on the vehicle, the impact angle depends on the local propeller geometry. For the critical location identified in subsection 4.3.2 this angle is 62°. When the propeller is not mounted the impact angle can vary.

The impact velocity for a tool dropped from 1.91 meter will be 6 m/s. This means the maximum perpendicular impact velocity and energy when mounted on the vehicle is 2.8 m/s and 11.8 Joule. When the propeller is laying on the floor the maximum impact energy is 54 Joule.

4.4.2. Runway Debris

The PAL-V Liberty will mostly take off from paved runways. These runways have debris on it. This is also called Foreign Object Debris or FOD. This FOD consists mostly out of parts of the runway or parts of other aircraft [65]. Asphalt, concrete, tar and paint make up FOD from the runway and metal, rubber and plastic make up FOD from aircraft.

The front tire of the PAL-V Liberty is positioned directly in front of the propeller as can be seen in Figure 4.6. This means that when the front tire lofts anything from the ground there is a chance that this piece of FOD will travel through the propeller disc. Which means there is a chance that the spinning propeller blade will hit this piece of FOD.

Figure 4.6: A Side View of the PAL-V Liberty in Fly Mode. image credit: PAL-V

One thing to consider is the lofting mechanism of the tire. A few mechanisms are considered by Schmidt [66]. Pinch lofting, hammer lofting, spin lofting and groove lofting. The first three mechanisms here will eject a piece of debris interfacing with the side of the tire. This could mean that these pieces will miss the propeller blade. Groove lofting will eject debris directly behind the tire. Groove lofting is when the tire rolls over a piece of FOD which is pressed into the grooves of the tire. The groove can then lift up the piece of FOD and throw it in the air as shown in Figure 4.7. Threat maps where created by Nguyen et al. [67] showing the impact areas on the bottom of transport aircraft, shown in Figure 4.8. This figure shows the relative probability of a piece of FOD thrown by the tires hitting a certain location on the underside of a C-130. Unfortunately PAL-V uses road tires on the aircraft. Road tires are different to aircraft tires. There is little known about the debris throwing characteristics of road tires but it is clear that these tires are also capable of throwing debris.

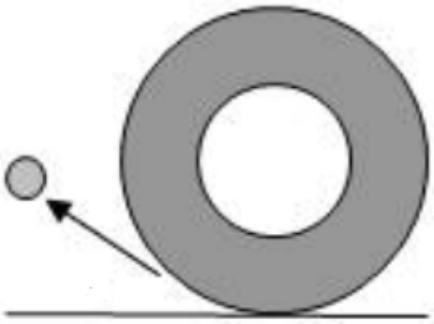

Figure 4.7: A Piece of FOD Ejected by Groove Lofting [67].

Another way to characterize the debris which can be thrown into the propeller is by looking at what is typically found on a runway. Herricks et al. [65] have analysed the FOD collected at a large commercial airport. It states that the average weight of the dangerous items found is between 9 and 18 grams depending on the runway. But unfortunately this has a standard deviation of 41 grams. This means the hazardous FOD can be as high 100 grams or even more. It is mentioned that 20% of the pieces are larger than 1 by 1 inch. A 1 inch (25.4 mm) cube of steel can weigh 130 grams. If a piece of FOD with this mass would ever be ejected from the road surface by the front tire is unknown. This could

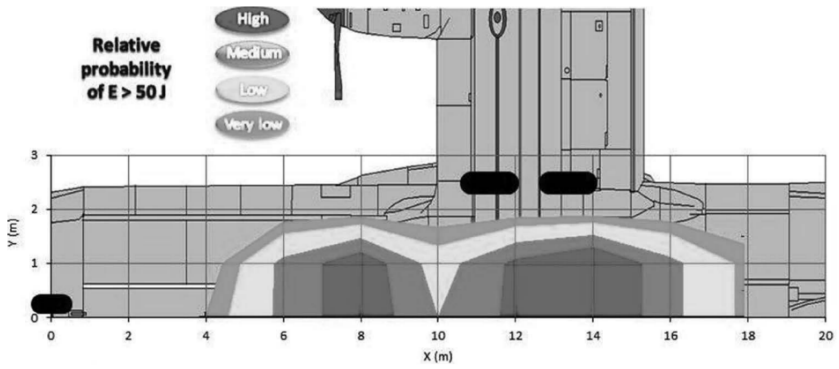

Figure 4.8: Impact Threat Map on the C-130 [67]

however be one of the physical tests still to be performed on the PAL-V Liberty test vehicle. PAL-V will also perform an analysis of the FOD found at Rotterdam The Hague airport to validate the results from Herricks et al. [65].

The maximum perpendicular velocity is 50 m/s on the critical location identified in subsection 4.3.2. When a piece of FOD weighing 130 grams would hit this location the perpendicular impact energy would be 162 Joule.

The current PAL-V Liberty test vehicle has already done some take-off rolls on a paved runway. It is apparent from these tests that FOD hitting the propeller is a realistic threat. The propeller used during these tests is shown in Figure 4.9. It can be seen that the propeller was hit by FOD and has chipped paint spots. This picture was taken after only 3 take-off runs.

Figure 4.9: FOD Impact on the PAL-V Liberty Test Vehicle. image credit: PAL-V

4.4.3. Bird Strike

The PAL-V Liberty will be certified according to CS-27 [6] for small rotorcraft with special condition SC-GYRO-1 [7]. To comply with these certifications it is only required to certify the aircraft for bird strike when it can seat 6 or more people. The Liberty will seat two people. The propeller will be certified according to CS-P [8]. On page 33 of this document it is stated that ”the Propeller is capable of withstanding the impact of the birds which are specified in the aircraft specifications *applicable to the*

intended installation of the Propeller." [8]. This means that the propeller does not have to be certified for bird impact.

It is however useful for this threat analysis to consider it. A bird according to CS-27 [6] will weigh 1.0 kg. However this is not an impact by a rigid body with a blund radius impactor. The bird is largely made of soft tissue which the propeller will cut through. This means the actual impact will be much less than for example in a drop tower with the same impact energy. The force is also distributed over a larger area. Park [68] used a solid model with a low E modulus as a substitute for modeling the entire bird. Computing the exact response of the blade would only be possible with a FEM model or physical tests as both the response of the bird and the response of the propeller are relevant. Another thing to consider was the fact that this thesis investigated BVID. A bird impact is considered a discrete source damage which is different to BVID.

4.4.4. Hail

The PAL-V Liberty will be certified for Day-VFR only. This means the aircraft is not allowed to operate within 1500m of any cloud horizontally [69]. An encounter with a hail storm is prohibited and therefor highly unlikely. If a PAL-V aircraft was to enter a hail storm it will be checked thoroughly and maintenance will be performed. It was however still useful to look at what hail impact could mean for the propeller as the aircraft can still be struck by hail while stationary on the ground.

The difficulty with hail was that it can become extremely dangerous in extreme cases. For simplicity the hail data from the Netherlands was used. It is known that once in 100 years a storm is recorded with hail up to 10 cm [70]. This 10 cm hail will have a terminal velocity of between 35 and 40 m/s [71] with a mass of around 500 grams. At the critical impact location from subsection 4.3.2 this means it has a perpendicular velocity of 19 m/s. This means the perpendicular impact energy is 90 Joule.

4.4.5. Foot Traffic or Luggage

When the vehicle is being loaded or unloaded, the people could bump into the propeller. This would be at a very low velocity. The propeller would be extended and stationary. In this state the propeller can actually move around the folding hinges and can rotate which would even further reduce the force applied to the propeller. It was not expected that this form of collision would cause any damage to the propeller.

4.4.6. Road Use

The PAL-V vehicle will also be used on the road. Although the speed is usually much lower on the road compared to flying, there are added risks. There are two main differences between the other impact cases and road use. The first difference is that the propeller is always folded in the road conditions, as shown in Figure 4.10. This will protect a very large part of the propeller from impact damage. The second difference is the fact that on the road, there are other vehicles and people in close proximity to the PAL-V vehicle. This can be another car which can loft FOD at the PAL-V vehicle while driving or even curious bystanders when the vehicle is parked.

The folded propeller is almost completely protected from damage. In Figure 4.10 it can be seen that the only part that is exposed is the inner part at the rear of the propeller this is however also the critical location identified in subsection 4.3.2. It can also be seen that the propeller is protected from the sides by the vertical stabilizers. This is more clearly visible in Figure 4.11. This leaves the exposed part of the propeller only accessible from the rear.

It seemed like the propeller cannot be damage during driving unless something small is thrown forward from another car. Even when rear ending the vehicle other parts would get hit first. A more likely way the propeller can be damaged on the road is when it is parked and something hits it by accident or on purpose. For example something being thrown around on the streets which hits the exposed section of the propeller. According to a study done by the CBS [72], 11.2-14.3% of all car owners were a victim of car vandalism between 1993 and 2005. It was still difficult to determine a specific weight and velocity of a projectile thrown by a vandal.

Figure 4.10: A View at the Folded Propeller in Drive Mode with the Exposed Propeller circled in Yellow. image credit: PAL-V

Figure 4.11: A Side View of the PAL-V Liberty in Drive Mode. image credit: PAL-V

One of the fastest objects thrown by people is a baseball. The record for a fastball stands at 47 m/s. With a baseball that weighs 140 gram that comes down to an impact energy of 156 Joule. This could very well be the limit of projectiles thrown. It is fair to say this is also the limit of throwing a stone or other hard object. A human can swing a 1 kg hammer at around 10 m/s [73] which would lead to an impact energy of 50 Joule. These are the most severe impact events possible due to vandalism.

4.4.7. Ground Service Equipment

Ground service equipment is used on larger aircraft to load for example passengers, fuel or luggage or equipment for de-icing or push-back. This sort of equipment is not used around the PAL-V Liberty. If a fuel service truck is used around the PAL-V Liberty, it will not be able to hit the propeller. In drive mode the propeller is tucked away as shown in Figure 4.10. When in fly mode, the propeller is protected by the rear wheels and the tail as shown in Figure 4.12.

Figure 4.12: Rear View of the PAL-V Liberty in Fly Mode. With a tooldrop scenario in purple. image credit: PAL-V

4.5. Frequency Analysis

The maximum impact energy that was expected also depends on the probability of that specific impact event happening. The Composite Materials Handbook [1] mentions that a maximum impact energy cut-off can be set at a probability of less than 10^{-9} per flight hour. This is considered "Extremely improbable failure conditions" in Advisory Circular 25.109-1A [74].

Kan et al. [11] have shown that 100 ft*lbs, or 136 Joule, can be considered the critical energy for BVID. This is considered a "very remote impact event for an in-service aircraft" [11]. The probability of occurrence is 0.1. How this relates to the probability per flight hour is not mentioned. This energy cut-off of 136 Joule was adopted by the industry [75]. This cut-off was analysed by Dubinskii et al. [75] in 2019 who proved that it is still a valid energy cut-off. This cut-off was utilized here for all impact threats when the propeller is stationary as this cut-off was determined for fuselage and wing structures. When the propeller is spinning the impact energy could be higher. When considering the spinning propeller, only runway debris is a threat and a frequency analysis can be useful to determine a cut-off.

An exact frequency analysis would mean a lot of data has to be available for this specific aircraft which wasn't the case. A rough estimate was however made using studies on different aircraft.

For a piece of runway debris to hit the propeller it has to be lofted in the right direction and hit by the spinning propeller blade. This piece also has to be large enough to inflict damage. Dubinskii et al. [75] have analysed the amount of impact damages on the wings of a wide variety of commercial aircraft. The Average probability of impact damage on the wing was $5.43 * 10^{-4}$ per flight hour. Herricks et al. [65] have shown that 20% of runway debris is larger than 1 inch by 1 inch which can easily be over 100 grams. From Figure 4.8 it is clear that most of the lofted debris is thrown behind the tire. The probability of a lofted piece of debris hitting a propeller blade when going through the propeller disk is 1 when the vehicle is stationary and reduces when the vehicle starts moving. These probabilities combined are probably not even near 10^{-9}. Unfortunately this was not enough to determine an energy cut-off. This meant that the best option for the energy cutoff was to use the 136 Joule industry standard.

4.6. Conclusion

The potential critical location identified in subsection 4.3.2 was 260mm from the root of the propeller blade on the back side of the propeller just before the spar transitions into the skin. The projectile sources shown in Table 4.1 clearly prove that the potential critical location identified in subsection 4.3.2 also has a significant impact threat. This proves that this location can be considered the most critical impact location on the PAL-V Liberty propeller. The industry standard energy cutoff is 136 Joule. This will also be the energy cutoff used by PAL-V.

Table 4.1: Impact Damage Sources with Perpendicular Velocity, Mass and Energy

Source	Perpendicular Velocity (m/s)	Mass (g)	Perpendicular Energy (Joule)
Tools	0-6	50-3000	0-54
FOD	12.5-50	0-130	0-162
Hail	0-19	0-500	0-90
Vandalism(throwing)	0-47	0-140	0-156
Vandalism(hitting)	0-10	0-1000	0-50

5

Detectability Threshold

Impact damage that leaves an indentation depth between 0 and the detectability threshold (DT) was considered BVID. It was thus clear that, for certification, impact damage is categorized based on detectability, as was found in subsection 2.2.1, and the detectability threshold will be based on indentation depth. The detectability of damage is the ease at which it can be detected. This chapter has set a minimal indentation depth at which impact damage will be reliably detected during maintenance inspections. This indentation depth is the DT which corresponds to the maximum BVID size. This is however the minimal impact damage size that was considered BVID when applied to the propeller blade prior to fatigue testing because for this test the worst case scenario has to be considered.

The DT along with a maximum was used as a range in which the impact damage applied to the propeller for fatigue testing is considered correct. The DT was set at an indentation depth with a Probability of Detection (PoD) of 90% with a 95% confidence level [1]. This means that if all the indentation depths of the damages with a PoD of 90% are put on a graph, the DT is the upper boundary of the interval which will capture 95% of the damages. It should be noted that when the damages are more easily detected, more of the damages will be detected. That means when the PoD for all damages is increased, the DT will be lower.

Doing a complete PoD study with a large number of impact damages and a large inspection group was considered highly unpractical for a rather small company like PAL-V in comparison to Boeing or Airbus. That is why literature was used to set the DT.

5.1. Previous Studies

The PoD is dependent on a lot of factors like indentation depth, damage diameter, inspection type, inspection distance, qualification of the inspector and substrate colour [15].

In the Composites Materials Handbook [1], the DT is assumed to be between 0.25mm and 0.60mm after relaxation. In Table 5.1, also shown in chapter 2, the values used by other companies are shown. The original sources of the publication of these values were hard to find. It was however clear that these values vary greatly. It was however noteworthy that the largest values in this table are from the US Air Force and the US Navy. The original source was not found and the reference trail leads to Rouchon [10] who mentioned that these are values used for military applications and not civil aviation. The trail ends at Kan. et al. [11] who mentioned the values but discarded them.

There is an ISO standard, ISO 18352:2009(en) [12], that sets the DT at 0.30mm.

Table 5.1: Comparison of Different BVID Values found in Literature. [13] [14] [15] [16]

Company	Aerospatiale	Boeing	Airbus	USAF	US NAvy	CAA
Detectability Threshold (DT), mm	0.3	0.25	0.3	2.5	1.25	0.25

Three more studies were found on the DT. These were all studies using a certain number of composite panels with defects in them. A group of people was then asked to visually inspect the panel and it was recorded if they detect the defect or not. This data was used to determine at what size the DT should be set according to each study. L Cook et al. [76] set the DT for a part with a gloss finish at 0.25mm, for Dubinskii et al. [14] this size was set at 0.30mm and Jiang et al. [15] found the DT at 0.33mm. These studies also found links between the DT and different factors like diameter, inspection distance, participant training, color and surface finish. The viewing distance was set at 1.2 meter [76], 0.7 meter [14] and 0.5 meter [15]. The following effects were found by and agreed upon by these three studies.

- Decreasing the viewing distance will increase the PoD
- A gloss finish will increase the PoD
- Dirty inspection conditions will decrease the PoD

5.2. The Detectability Threshold for the PAL-V Propeller

To select the DT for the PAL-V propeller, it was important to look at the inspection conditions. The propeller can be inspected from a distance less than 0.5 meter because the propeller is mounted at eye level. The propeller will also have a gloss finish. The maintenance inspection will always be performed by trained maintenance personnel and in a controlled environment.

When the ISO DT value of 0.30mm was considered, only three of the mentioned sources have a higher DT. The US Air Force, the US Navy and Jiang et al. [15]. The US Air Force and US Navy values were discarded due to the questionable reference trail and a different application field. Jiang et al. [15] put the viewing distance at 0.5 meter.

It was deemed sufficient to set the DT at the same level as the ISO 18352:2009(en) value of **0.30mm** indentation depth if the following procedures are followed:

- The propeller will be inspected by trained maintenance personnel during periodic inspection
- The propeller will be cleaned prior to inspection
- The viewing distance will be less than 0.5 meter

6

Coupon Testing

ASTM D7136 impact testing is a testing standard that is widely used in the industry. Often as a preparation for Compression After Impact (CAI) testing. This means that material testing facilities often already have the required equipment to perform the tests. These ASTM D7136 impact tests were used to map the structural response of the coupons to impact loading. After that, quasi-static indentation testing was used on the coupons to map the differences in structural response between impact loading and quasi-static loading. This chapter explains the setup, results and conclusions of the ASTM D7136 impact tests as well as the coupon quasi-static tests.

In section 6.1 the test setup is explained for the impact tests and for the quasi-static tests along with the design and fabrication of the test coupons. The results are presented in section 6.2 and the verification of these results is explained in section 6.3. In section 6.4 it is explored what information was gained from the results.

Figure 6.1: A Coupon Sample in the Compression Test Bench

6.1. Setup

The complete test setup for the impact tests was already described in ASTM D7136 [46]. This section explains this test setup in general but provides more detail on the coupons and load cases during the impact tests as these were specific to this research.

The ASTM D7136 [46] setup was also mimicked for the quasi-static coupon tests. This meant the same coupon fixture was used with the same loading tip at the contact location. The test setup is shown in Figure 6.1.

6.1.1. Coupons

The coupons required for testing are specified by the size stated in ASTM D7136 [46] and the structure of the propeller at the critical location determined in subsection 4.3.2. The coupons were cut out of two 679x679 mm flat plates. A flat aluminium plate was used as a tool on which the plates were laminated. The laminates were backed by a caul plate.

Materials

The materials used for the coupons are the same materials used in the PAL-V propeller. It was produced from prepreg carbon fiber. The exact details on the materials are confidential and are not discussed in this report. The propeller has a copper mesh outer layer for lightning protection which was be included in the coupons.

Layup

The layup of the coupons was the same as the skin layup in the propeller at the critical location. The copper mesh was placed as the first layer on the aluminium tool. The laminate was debulked after every few layers of prepreg composite material. The required 679X679mm sheets fit on the roll diagonally to create the 45 degree fabric layers. Because the prepreg fabric had to be used efficiently, the triangular off-cuts created in this process were also used to create the 45 degree fabric layers. This resulted in one plate being produced with continuous layers and one plate with a butt-joint diagonally across the plate in most 45 degree fabric layers. These butt-joints were aligned to concentrate these imperfections to one line which meant most coupons remained unaffected.

Curing

The aluminium tool with the two laminates and caul plates was topped by a layer of breather and a vacuum bag. The plate was kept under vacuum for a certain time before curing. The exact manufacturers cure cycle was followed.

Cutting

After curing the plates were cut into 150x100 mm coupons as specified in ASTM D7136 [46]. The cutting diagram is shown in Figure 6.2. The plates were cut using a water cooled circular diamond saw.

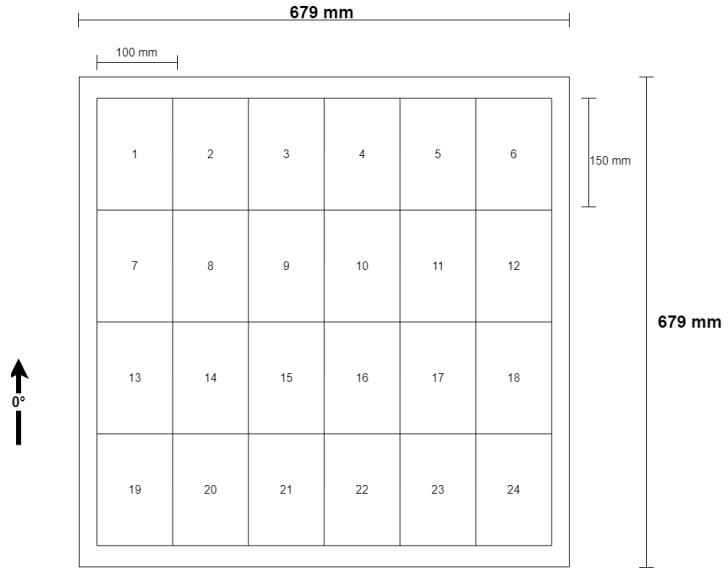

Figure 6.2: Plate Dimensions and Cutting Diagram (679x679mm)

Yield

A total of 48 coupons were cut from the two 679x679 mm plates. Unfortunately not all coupons were of the same quality. The coupons were numbered, evaluated and graded to categorize them into different qualities. The edge defects were larger than expected which significantly reduced the thickness of the coupons near the plate edges. The coupons with a butt-joint in the 45 degree fabric layers were also marked. This butt-joint along with other defects like size defects or folds in the copper mesh resulted in the coupons being divided into 4 categories. Perfect, usable, bad and unusable. The amount of coupons in each category is shown in Table 6.1. A coupon mounted in the ASTM test fixture can be seen in Figure 6.4

1. Perfect coupons were used to create the most critical data points.
2. Usable coupons have a small defect which was not expected to influence the results. For example a small thickness variation across the short side or a butt-joint in the 45 degree fabric layer which is not near the impact zone. These coupons were used for important data points.
3. Bad coupons were expected to have defects which influence the results. This can be a thickness variation on the long edge of the coupon or a butt-joint in the 45 degree fabric layers underneath the impact zone. These coupons were only used for tests which were not used for making a prediction.
4. Unusable coupons are coupons which do not meet the standard at all. They were still used as dummy coupons for trial runs to ensure proper functioning of test equipment.

Table 6.1: Amount of Coupons in each Quality Category

Quality	Amount
Perfect	14
Usable	16
Bad	9
Unusable	9

6.1.2. Drop Tower

ASTM D7136 [46] specifies the use of a drop tower to apply the impact loading to the coupons. The drop tower used is located inside the DASML mechanical testing hall at the TU Delft. This drop tower is shown in Figure 6.3

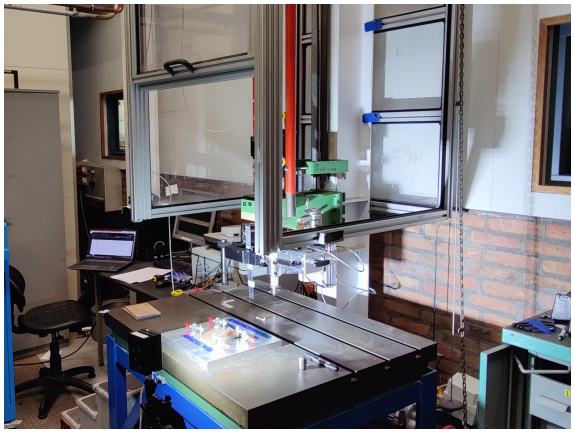

Figure 6.3: The Drop Tower used for ASTM Impact Testing.

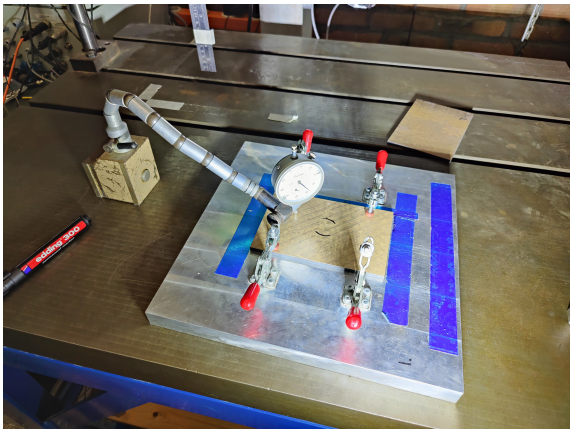

Figure 6.4: A Coupon in the ASTM Test Fixture.

Functioning

The drop tower consists of a sled on a vertical track and a table. The sled is hoisted to a certain height by a carriage with an electrically operated hook. The impact loading will be applied by a dart which is released from the sled just before impact. This dart has a 16mm radius semicircular tip in accordance with the test standard. The mass of the dart can be adjusted by adding or removing discs. After the impact event the dart is captured by a catch mechanism to prevent a second strike onto the test piece.

Coupon Fixture

The 100x150 mm coupons were placed on a plate with a 75x125 mm rectangular hole. The coupon was held down by 4 toggle clamps with rubber tips. This plate was lined up underneath the drop tower with the dart lining up to hit the centre of the coupon. This plate with a coupon and a dial indicator is shown in Figure 6.4. The same coupon fixture was used for the quasi-static coupon tests.

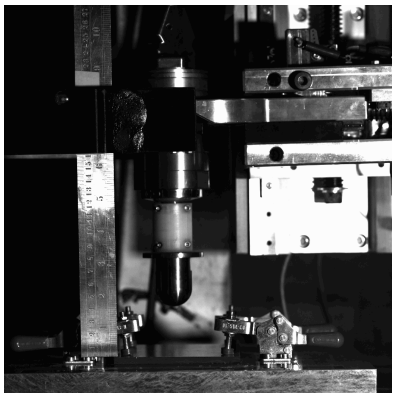

Figure 6.5: A Still Image of the Velocity Measurement Video.

Figure 6.6: The Dial Indicator used for Dent Depth Measurements

Measurements

The data that was required for these tests was the impact energy, contact force and the indentation depth after the impact. The impact energy was calculated with the mass of the dart and the impact velocity. The mass of the dart was measured at the start of the experiments using a scale. The velocity was measured before and after impact using a high speed camera and a ruler which was placed next to the dart. A still image of this high speed camera is shown in Figure 6.5. The contact force was measured using a load cell inside the dart and recorded at 500 kHz. After the tests were performed it unfortunately became clear that in the preamplifier for the load cell a 1 kHz low-pass filter was applied. This meant any information in the contact force data happening at a higher frequency was filtered out before the data even reached the computer. The indentation was measured using a dial indicator, shown in Figure 6.4 directly after the impact event.

6.1.3. Compression Test Bench

The machine used for compression testing was an Instron 5989 universial testing system [77]. It has a maximum load of 600 kN but was primarily chosen for the large specimen capacity to accommodate the propeller as the same machine was used for coupon and propeller quasi-static testing. Displacement and load measurements came directly from the sensors integrated in this testing system. As mentioned before the coupon fixture for the ASTM D7136 tests was placed in this compression test bench and a 16mm hemispherical tip was used to apply the load.

6.1.4. Load Cases

The two factors that could be altered to control the impact energy during the impact tests were the mass and drop height of the dart. To achieve the impact levels necessary the highest possible mass for the dart was selected at 4.94 kg.

Impact energies were selected to create a complete relation of impact energy and dent depth with corresponding contact force data. The impact energy that was of interest the most was the impact that causes BVID after relaxation. Which corresponds to, according to chapter 5, a dent depth of 0.30 mm. Relaxation extends this area of interest to higher energy levels. That is why the dent depths between 0 and 1mm were the aim and for the impact energies that cause BVID the best coupons were used.

The impact energy required for a certain indentation was determined by trial and error. The impact energy can't be controlled directly and the influence of the sled on the dart was unknown. That is why the drop height was set at 1 m for the first drop and varied up and down until the area of interest was filled with data points. In the end 29 impact tests were performed ranging from 27.8 to 65.6 Joule

The loading rates for the quasi-static tests were selected based on the amount of tests that needed to be performed and the time available on the test machine. These rates were set very slow to mirror quasi-static loading.

The coupons were loaded at 2mm/min until a certain load was reached. For the first tests this maximum was 8 kN after which the coupons were also unloaded at 2mm/min. For the second set of tests the maximum was set higher than the ultimate strength and the test was stopped after 8 mm of displacement.

6.1.5. Relaxation

As mentioned in subsection 2.3.1 the indentation after impact will relax over time. This was also measured and recorded. Unfortunately the measurement setup used directly after impact was unavailable after the impact tests and a secondary method was used. This secondary method also uses a dial indicator but it takes a reference from the edges of the coupons, as shown in Figure 6.6, not the base of the ASTM fixture plate. This was only measured on the coupons that were used for the impact tests.

6.2. Results

The results for the coupon tests are presented in this section.

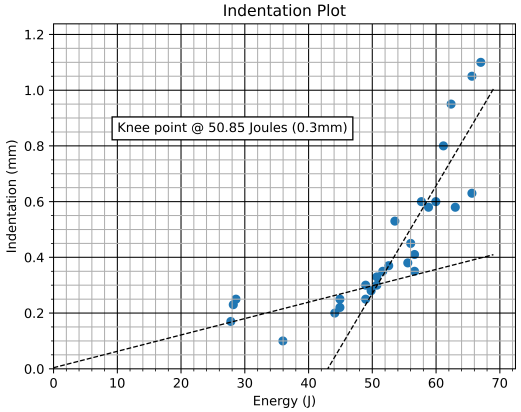

Figure 6.7: Indentation vs Energy plot with Knee point.

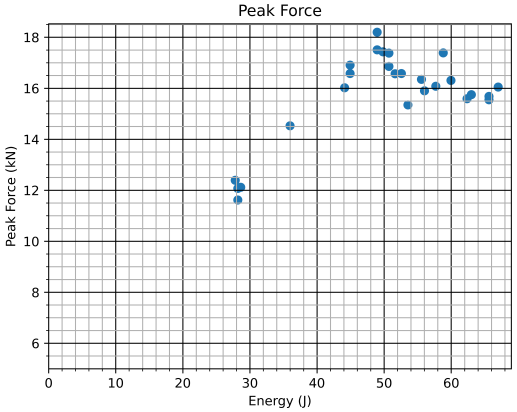

Figure 6.8: Peak Force vs Indentation

6.2.1. ASTM D7136 Impact Testing Results

The raw data points are shown in Appendix A. From this data four plots were made to visualise the data. In Figure 6.7 the indentation depth was plotted versus the impact energy. The peak force recorded during the impact events was also plotted versus the impact energy in Figure 6.8. To further characterise the impact events that cause an indentation in the BVID range, the contact force during some of the impact events were plotted. For comparison some of the impact events were grouped into low, BVID and high indentation. Impact events that create an indentation between 0.17 and 0.25 mm were considered low indentation, an indentation between 0.3 and 0.35 mm was considered BVID indentation and an indentation between 0.95 and 1.10mm was considered high indentation. The contact force for Low indentation versus BVID indentation was plotted in Figure 6.9 and BVID indentation versus high indentation was plotted in Figure 6.10.

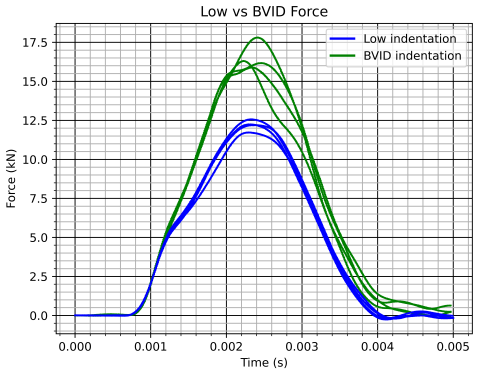

Figure 6.9: Force Plot of Low and BVID indentation impacts

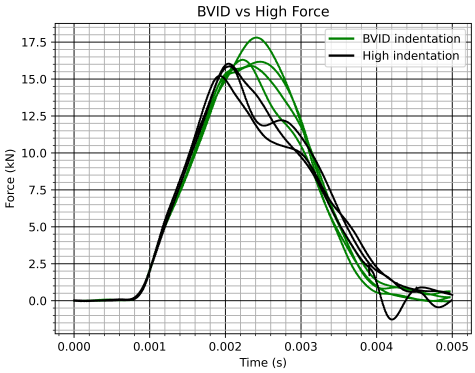

Figure 6.10: Force Plot of BVID vs High indentation impacts

Unfortunately the drop tower broke twice during operation at a high impact energy. This was caused by the large impact energy events. In one instance the vibrations of the impact event caused one of the wires of a trigger mechanism to break which resulted in the computer not initiating the data collection and the catch mechanism. In the second instance the catch mechanism sheared of at the attachment point to the rest of the tower. This was caused by the high rebound energy and the absence of damping on the catch arm.

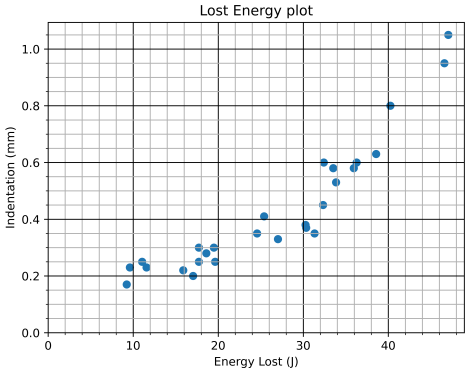

Figure 6.11: The Energy Lost during an Impact Event

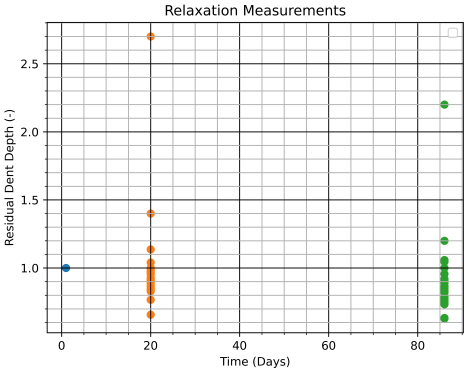

Figure 6.12: Residual Dent Depth Measurements.

6.2.2. Relaxation Results

The dent depth was measured directly after impact, after 20 days and after 86 days. As mentioned in subsection 6.1.5 the measurement method changed after the first measurement. This can have a large impact on the outcome. The results of these measurements are shown in Figure 6.12. Here the depth measurement at 20 and 86 days were divided by the initial dent depth. This made a direct comparison of different initial dent depths possible.

6.2.3. Coupon Quasi-static Test Results

The results from the coupon quasi-static tests are shown in Figure 6.13 for the 8 kN tests and in Figure 6.14 for the ultimate strength tests. There were no anomalies during the coupon quasi-static tests.

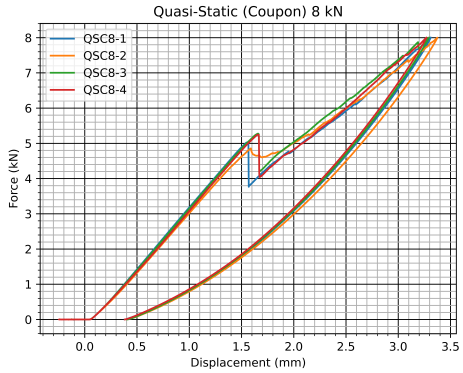

Figure 6.13: Force Displacement of Quasi-static Coupon Loading (8kN)

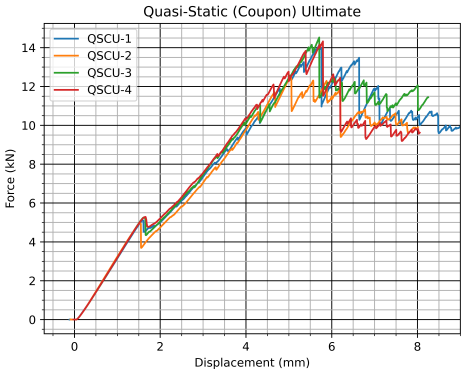

Figure 6.14: Force Displacement of Quasi-static Coupon Loading (Ultimate)

Table 6.2: Momentum change and Impulse calculation for ASTM D7136 Impact Testing

Impact Nr.	$M * \Delta V$	$F * t$	**Ratio**
1	35.82	26.95	0.75
3	35.48	27.73	0.78
4	38.14	29.59	0.78
5	36.56	29.02	0.79
6	38.06	30.13	0.79
7	37.46	30.45	0.81
8	35.89	28.53	0.79
9	38.18	30.53	0.80
10	36.19	28.88	0.80
11	37.75	30.10	0.80
12	35.55	27.49	0.77
13	38.24	29.37	0.77
14	38.06	29.94	0.79
15	36.25	27.99	0.77
17	38.43	29.28	0.76
18	38.40	30.41	0.79
21	28.83	21.64	0.75
22	28.37	21.39	0.75
23	28.97	22.27	0.77
24	29.08	22.15	0.76
25	37.33	28.55	0.76
26	40.21	30.21	0.75
27	37.51	29.04	0.77
28	39.71	30.39	0.77
Average Ratio		**0.78 (SD=0.018)**	

6.3. Result Verification

To verify the force history plots from the impact tests in section 6.2, a simple calculation was done. The change in momentum of an object is equal to the impulse of the force exerted on that object [78]. This simple equation is shown in Equation 6.1. The impact and rebound velocity was taken from the high speed footage and the force history, like the ones shown in Figure 6.10, was used to calculate the impulse. The results are shown in Table 6.2, with an average ratio and a standard deviation. From this it was clear that there was a considerable difference. It seems like the force measured by the load cell was smaller than it really was.

$$J_i = F * t = M * \Delta V = p \tag{6.1}$$

To verify if this method of comparing impulse to momentum change is actually valid the same was done on completely different impact data. PAL-V has done impact testing on the propeller before at the NLR. This means it was the same material and similar layup but on different locations with a different thickness. This data was used to perform the same impulse calculations as in Table 6.2. The results of this calculation are shown in Table 6.3. These values show that calculating impulse through the force history and comparing this to the change in momentum should result in the same values.

To find the issue, the calibration of the load cell on the drop tower used for ASTM impact testing was verified and found to still be valid. To exclude the 1 kHz filter as a cause of this difference the same 1 kHz filter was applied to the force history of the NLR impact tests which yielded very similar results. These values are also shown in Table 6.3.

A second check was done to explore this difference further. From Figure 6.8 it is clear that after the knee point the peak force levels out and never exceeds 18 kN. Because the NLR impact tests were done on the same material but with a thinner total layup it was expected that the impact force history plots created after the NLR impact tests would also not exceed 18 kN. The peak force for the NLR impact tests is also shown in Table 6.3. This peak force was taken from the data with the 1 kHz filter applied to mimic the peak force found in Figure 6.8. It was clear that these values are higher than the maximum of 18 kN found at the ASTM coupon impact tests. Although this was not an accurate comparison as the NLR impact tests were done on a thinner section of the carbon fiber it was an indication that the force history results from the coupon tests were wrong. One would expect a lower peak force on the thinner material but Table 6.3 clearly shows the opposite.

After this verification it was decided that even though the error was not found in the drop tower at the TU Delft, there was enough ground to assume that the force history was wrong. It was decided that the inverse of the average ratio found in Table 6.2 would be used as a correction factor for the force history results from the TU Delft drop tower. This correction factor was **1.282**. The plots shown in section 6.2 were corrected by this value and are shown in Figure 6.16, Figure 6.17 and Figure 6.18. This correction has ensured the impulse calculation follows simple physics and the peak force found makes sense compared to the peak force found at NLR impact testing. This correction factor was proven once more in subsection 8.2.2.

Table 6.3: Momentum change and Impulse calculation for NLR Impact Testing

Impact Nr.	M*DeltaV	F*t	Ratio	F*t (1kHz)	Peak Force (1kHz) (kN)
WBA-I	40.78	40.43	0.99	40.46	19.6
WBA-HI	40.69	40.25	0.99	40.29	19.4
WBV-I	45.20	44.87	0.99	44.91	20.0
WBV-HI	45.52	45.32	1.00	45.35	19.5

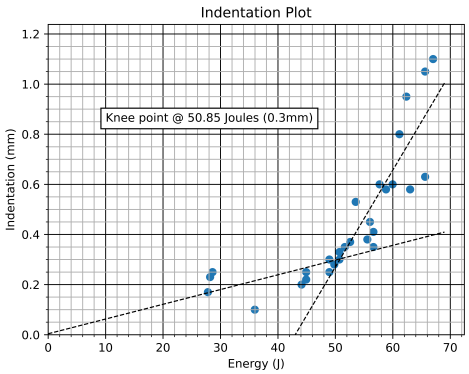

Figure 6.15: Indentation vs Energy plot with Knee point.

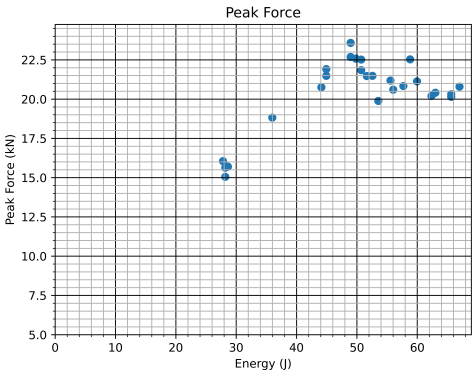

Figure 6.16: Peak Force vs Indentation (Corrected)

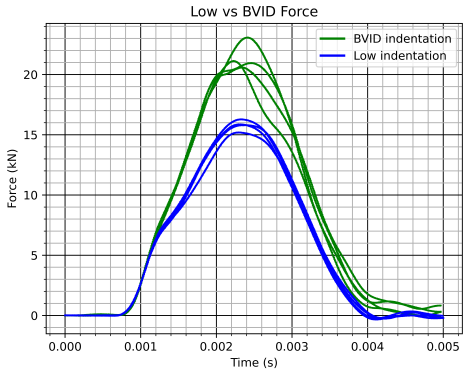

Figure 6.17: Force Plot of Low and BVID indentation impacts (Corrected)

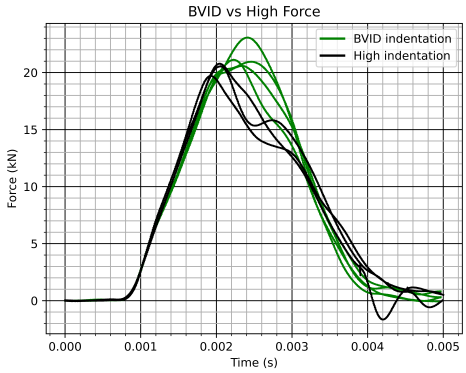

Figure 6.18: Force Plot of BVID vs High indentation impacts (Corrected)

6.4. Discussion

A lot could be learned from the coupon testing results. The findings from all the coupon tests is discussed below.

6.4.1. Discussion on Coupon Impact Tests

It was expected to find a knee point in the indentation versus energy plot shown in Figure 6.7. This knee point was found at 50.85 joule at an indentation depth of 0.30mm. This coincidentally was right on the detectability threshold found in chapter 5. When looking at Figure 6.16 this knee point was also visible. Up until 50 joule the peak energy seems to be linearly related to the impact energy. Above the knee point the peak force is no longer increasing linearly with the impact energy and a maximum peak force was reached.

In Figure 6.17 the impact events creating low indentation and a low peak force are shown to have a kink right around 6 kN. This probably was the point at which the first damage initiates. The BVID indentation force plots clearly differ. The BVID indentation plots show a steeper climb of the contact force corresponding to the higher impact velocity. It was clear that to cause significant damage, BVID or higher, a contact force threshold of 20 kN needed to be reached.

From Figure 6.18 it was also clear that above the knee point, the peak force does not increase further. The higher indentations once again show a steeper climb corresponding with the higher impact velocity. The higher indentations were characterised here with a steep drop right after the peak force indicating the coupon was more damaged after the peak compared to the BVID indentation plots.

The impact events all took around 3 ms. When comparing this impact duration to the 1 kHz filter mentioned in subsection 6.1.2 it became clear that this low-pass filter had probably removed some interesting information that could be gained from the force plots.

6.4.2. Discussion on Relaxation

When looking at the relaxation results shown in Figure 6.12 it was immediately clear that the dent depth measurements have not been completely accurate. The dent depth seemed to increase for some data points which indicate either an error made while reading the dial indicator or, more likely, a clear difference between the two used measurement methods mentioned in subsection 6.1.5. To make some sense of the measurements first the outliers were removed from the data. This is shown in Figure 6.19. These data points were used to calculate the mean with the confidence interval shown in Figure 6.20. As mentioned in subsection 2.3.1 the expected shape of these relaxation results was a logarithmic fit. A logarithmic fit was also applied to the means values and shown in Figure 6.20. The relaxation relation found by Dubisnii et al. [14] is also shown as a reference. These logarithmic approximations were plotted to 300 days in this graph to predict further relaxation of the dents. Even though it seems fair to say that the residual dent depth would be 75% to 80% of the original dent depth after a year, more relaxation measurements have to be performed more consistently to form a proper prediction of the relaxation. If this estimate proves to be correct after more measurements the initial dent depth for BVID would be **0.375-0.40 mm.**

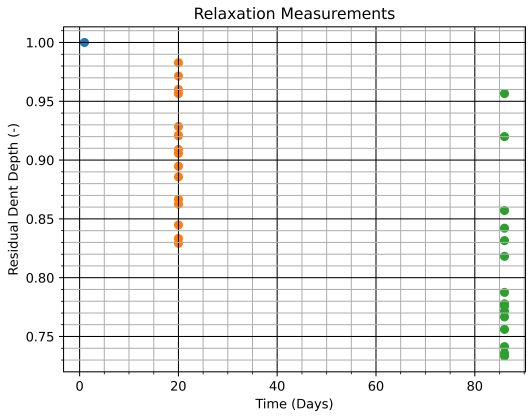

Figure 6.19: Residual Dent Depth Measurements. Without Outliers.

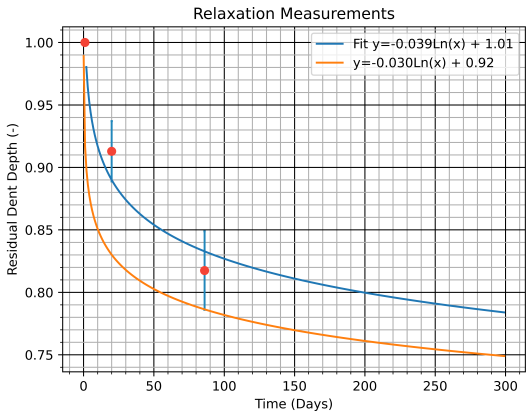

Figure 6.20: Mean, Confidence interval and Logarithmic fit of the Relaxation results.

6.4.3. Discussion on Quasi-static Coupon Testing

The first thing to notice from the quasi-static tests was the fact that the coupons seem to perform very similar. No large deviations in stiffness or even ultimate load was visible in the results. The coupons all had a very distinctive first failure at 5 kN and an ultimate load between 12.5 and 14.5 kN. These values were lower than the values found in impact testing. The first failure seemed to happen at 6 kN in impact testing and ultimate loads were also way higher at 20 to 23 kN. This indicates different structural behaviour at different loading rates.

One input that was used for the prediction model was the spring constant. This spring constant was estimated by performing a linear fit on the first, undamaged, part of both the coupon loading diagrams. The results are shown in Figure 6.21.

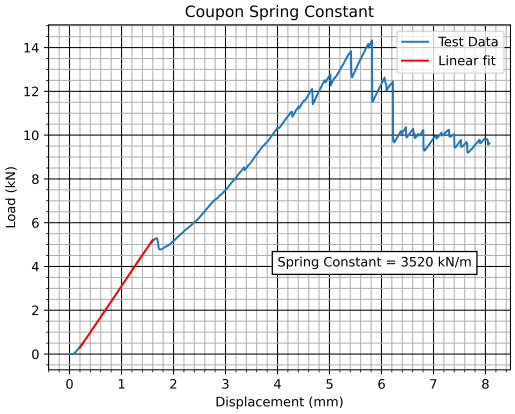

Figure 6.21: Spring constant estimate of Coupons by Linear Fit

7

Propeller Quasi-static Indentation Testing

In this chapter the propeller quasi-static tests are explained. The goal of this test was to determine the structural response of the propeller to quasi-static loading. This response was later used to create the model for impact damage prediction.

In section 7.1 the test setup and load case is explained. In section 7.2 the results are presented after which the results are discussed in section 7.3.

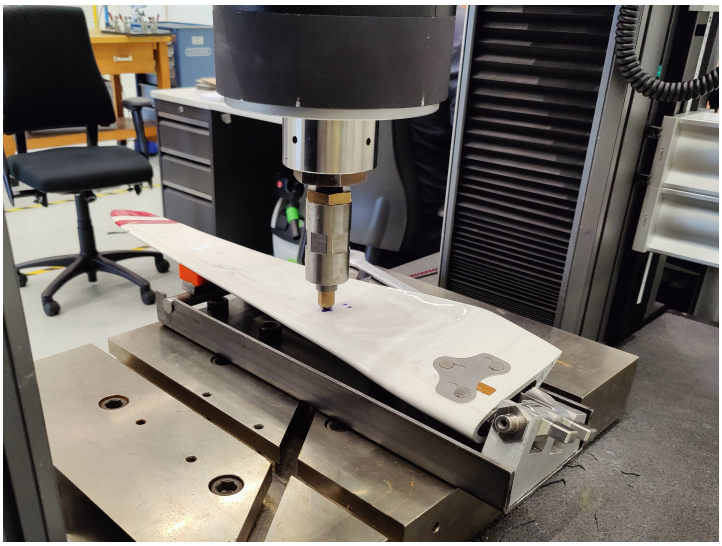

Figure 7.1: The White Propeller in the Compression Test Bench

7.1. Setup

The same Instron 5989 universal testing system [77] was used as for the quasi-static coupon test from subsection 6.1.3. The fixture for the propeller was designed and constructed for this test. This is explained in subsection 7.1.2. The test setup is shown in Figure 7.1.

7.1.1. Propellers

Two propellers were available for testing. A white and a black propeller. Unfortunately both propellers had already been damaged previously.

The white propeller was already used on the PAL-V Liberty test vehicle. There were numerous small chips in the paint on the leading edge. These paint chips did not seem significant to the structural

health of this propeller. This propeller was however also used for previous impact tests under a drop tower. This has left numerous indentations ranging from 0 to 1.9mm indentation depth. The trailing edge of this propeller has also been split open during these impact tests.

The black propeller has been used in lightning tests. Clear burn marks were visible where the lightning struck the propeller and where the propeller was connected to ground at the hub. It did however seem that this was only local damage at the two mentioned locations. The copper mesh that conducts these currents on the outside had not been damaged anywhere else. The propeller probably had better structural health than the white propeller blade. That is why this propeller was loaded with caution during these quasi-static tests to keep it structurally in the same condition for the propeller impact tests.

7.1.2. Propeller Fixture

To hold the propeller in the quasi-static test bench a purpose built fixture was designed and built. The fixture was designed to hold the propeller in a way that the critical location determined in subsection 4.3.2 is perfectly horizontal. The propeller had to be placed in a way that mimics the real scenario.

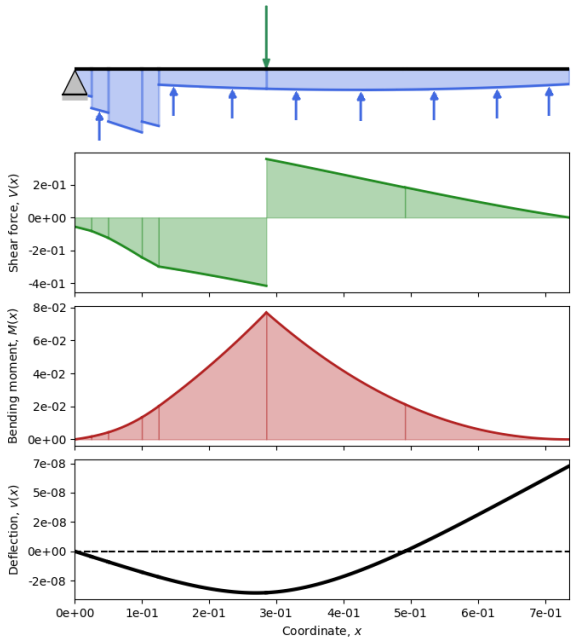

Figure 7.2: A Simple Beam Model to approximate the Rotating Propeller.

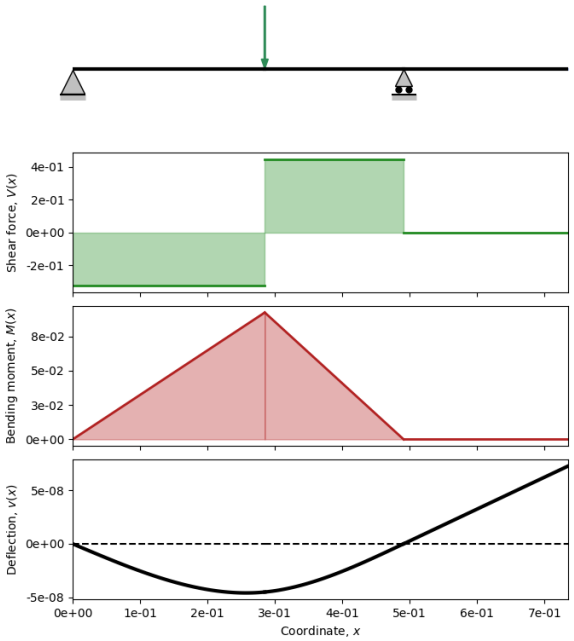

Figure 7.3: A Simple Beam Model to approximate the Propeller Fixture

Boundary Conditions

When the propeller is struck by FOD, the propeller will be spinning. This set of boundary conditions is very hard to reproduce underneath a drop tower. That is why a different set of boundary conditions was used and compared to the rotating case. The root side of the propeller was constrained exactly like the real case. The propeller was attached to the lug and the lug was held in place with a pin. In the rotating configuration, the centrifugal loads caused when the propeller hinges slightly out of the rotating plane, will provide the moment that will counter the applied load on the impact location. A simple beam analysis of case is shown in Figure 7.2. To approximate these conditions, it was decided to provide a roller support somewhere along the span of the propeller. In the design documents provided by the propeller manufacturer a modal analysis is provided. In this analysis a clear node is present at 490 mm from the hinge. In this location the roller support was also applied to allow the propeller to oscillate in the same mode. A beam analysis of this case were the propeller is pinned at the root with a roller along the span is shown in Figure 7.3.

The absolute numbers in Figure 7.2 and Figure 7.3 are not relevant but the comparison of the two lets us compare the two cases. The moment created by the rotation of the propeller was approximated

by the distributed load shown in blue in Figure 7.2. This was simply the local mass of the propeller multiplied by the rotational acceleration. The approximation in Figure 7.3 is exactly the same configuration as shown in Figure 7.2 but without the distributed load. This means the roller will provide the counteracting moment.

When comparing the two cases, the approximation experienced a bending moment that is 20% higher than the real case. The negative shear forces were 22% lower in the approximation and the positive shear forces were 26% higher in the approximation. Although the negative shear force was lower in the approximation, it was still considered a sufficient approximation of the real case. Second to the local damage caused by the impact, the bending moment was expected to inflict the most internal damage to the propeller and this bending moment was not reduced in the approximation. That is why it was chosen to support the propeller with the lug and a roller.

Design

A propeller fixture was designed to hold the propeller with the supports determined in the previous section. A key factor in this design was the fact that the critical impact location was oriented perfectly horizontal. This design is shown in Figure 7.4. When the impact location was located underneath the compression test bench the hinge location of the propeller lug was unsupported by the compression bench work table. That is why the supporting structure was make out of a U-profile steel beam to minimise displacement in the vertical axis. The support block which supports the propeller lug was made out of aluminium for ease of machining as this block needed to be machined in a mill to provide the lug support at the right angle. The roller support was made out of a steel pin on which a steel spacer was placed which was allowed to slide on the steel pin. To support the propeller in this location a 3D printed adapter was made which follows the propeller blade profile which distributes the load to prevent a point load from locally damaging the propeller. The U-profile beam was bolted down to t-slots in the compression bench work surface. The final result can be seen in Figure 7.1

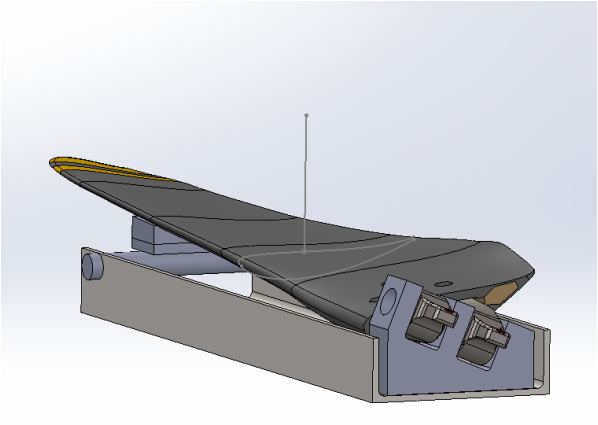

Figure 7.4: ISO view of the Propeller Test Fixture with Propeller and Lug

Analysis

To ensure that the deformations in the propeller fixture would not influence the test results a FEM analysis was done in ANSYS. The reaction forces when the propeller is loaded in the impact location was determined by considering the maximum contact load found in section 6.2 of 23 kN and dividing that in two reaction forces. This resulted in a vertical reaction force of 9.66 kN at the propeller lug and 13.34 kN at the roller pin. These reaction forces were applied to the aluminium block and the holes which will support the roller. The angle in the aluminium block further divided this load into a bearing load of 8.89 kN and a thrust force of 3.78 kN on the two sides constraining the propeller lug. The deflection in the vertical direction was the most important result to make sure that the deformations in the fixture don't influence the test results. The maximum deflection was 0.15mm at a load of 18 kN. The load case and illustrations of this analysis can be found in Appendix B.

7.1.3. Compression Test Bench

The machine used for compression testing was an Instron 5989 universial testing system [77]. This is the same machine that was used for coupon quasi-static testing. Displacement and load measurements came directly from the sensors integrated in this testing system.

7.1.4. Load Cases

Similar to the coupon quasi-static tests, the loading rates were selected based on the amount of tests that needed to be performed and the time available on the test machine. These rates were set very slow to mirror quasi-static loading.

The propellers were loaded at 2mm/min until a certain load was reached. The white propeller was loaded until 2, 3 and 4 kN. The black propeller was loaded twice to 1 kN to prevent any major damage from occurring.

7.2. Results

In Figure 7.5 the results for the white propeller tests are shown and in Figure 7.6 the results for the black propeller tests. Just like in the coupon quasi-static tests, there were no anomalies when performing these tests.

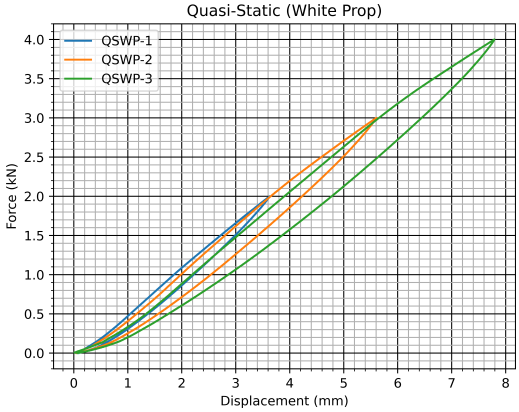

Figure 7.5: Force Displacement of Quasi-static White Prop Loading

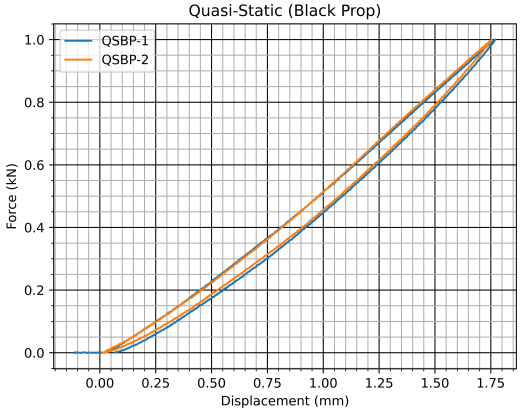

Figure 7.6: Force Displacement of Quasi-static Black Prop Loading

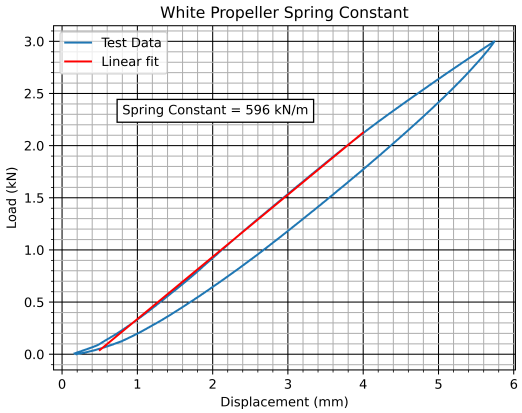

Figure 7.7: Spring Constant estimate of Prop by Linear Fit

7.3. Discussion

One input that was used for the prediction model was the spring constant. This spring constant was estimated by performing a linear fit on the first, undamaged, part of the propeller loading diagrams, just like the spring constants for the coupons. The results are shown in Figure 7.7.

As mentioned in subsection 7.1.1, there was a difference in pre existing damage in the white propeller compared to the black propeller. This however was not clearly visible in the response until 1 kN. A comparison is shown in Figure 7.8. In this figure there is an offset present in the displacement to better compare the two lines. The stiffness in this section was 604 kN/m for the white propeller and 613 kN/m for the black propeller. The line for the black propeller does seem to be stiffer more towards the 1 kN load but unfortunately the black propeller was not loaded any further and it is not known if the black propeller has a different structural reaction at a higher load. During testing it was clearly visible that the trailing edge of the white propeller opened up at higher loads. This is shown in Figure 7.9. One could assume that if the black propeller has an intact trailing edge this would mean a stiffer reaction at these higher loads.

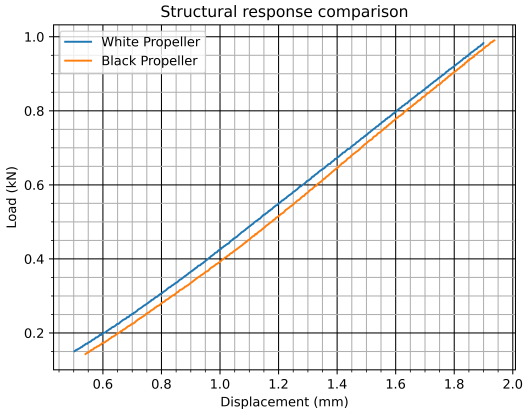

Figure 7.8: Structural Response Comparison of the White and Black propellers.

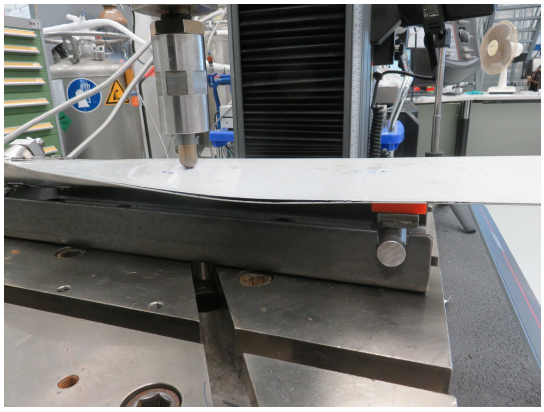

Figure 7.9: Opening of the Trailing Edge of the White Propeller.

8

Contact Force Prediction

In chapter 6 it was determined that a 20 kN contact force has to be reached to initiate significant impact damage. In this chapter a model is presented that aims to predict when the contact force reaches this 20 kN threshold.

The layout and physics of the model are explained in section 8.1 along with the basics of the program which ran this model. The parameters used in the model and how they were determined is shown in section 8.2. The results of the model are presented and discussed in section 8.3 and section 8.4.

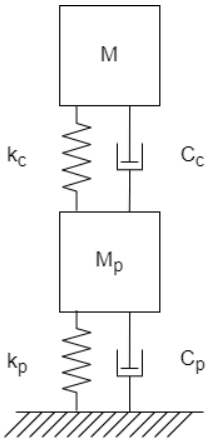

Figure 8.1: A two mass Impact Model

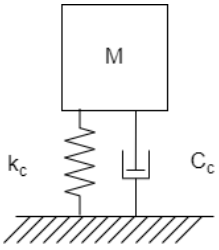

Figure 8.2: A single mass Coupon Impact Model

8.1. Two Mass Model

In subsection 2.4.1 a spring and mass model with two masses was introduced for boundary controlled impact. This type of model was used for the propeller impact prediction as well. Two dampers were added to account for internal dampening in the propeller and in the contact. A Python program, which uses this model, was written with which the results were calculated.

The first mass was the mass of the impactor or dart. The contact stiffness was approximated by the coupon stiffness. The second mass was the local mass of the propeller. The spring constant for the propeller was determined by combining the overall spring constant for the entire system and the contact stiffness. M and M_p are the mass of the impactor and the local mass of the propeller. k_c and C_c are the spring constant and damping coefficient of the contact while k_p and C_p are the spring constant and damping coefficient of the propeller. This model is shown in Figure 8.1.

The model works by evaluating the position and velocity of the two masses at small time intervals. The model starts with the dart having a certain initial velocity which was the impact velocity of the dart. After one time step the positions of the masses are updated which correspond to a certain displacement in the springs and a certain velocity in the dampers. This results in a force being applied to the masses which in turn causes an acceleration of the masses. The change in velocity of the masses by this acceleration is subtracted from the previous velocity and the model is repeated for the next time step. A block diagram is shown in Figure 8.3.

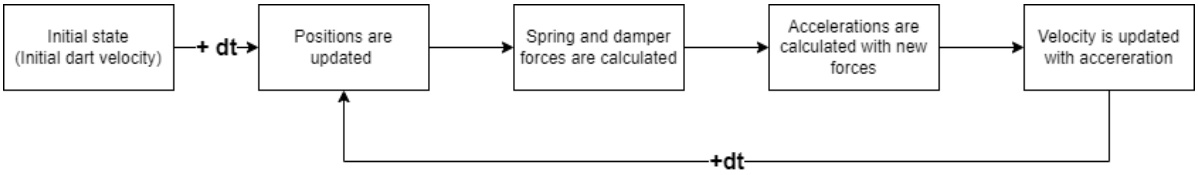

Figure 8.3: A Block Diagram of the Workflow of the Prediction Model

8.2. Model Variables

In this section the variables of this two mass model were determined. It is important to note that the methods explained below for determining the spring constant and damping coefficient influence each other. The results in the sections below already take into account the results of the other sections.

8.2.1. Local Propeller Mass

The local propeller mass is the effective mass of the propeller at the impact location. This local mass can be approximated by looking at the spring constant of the propeller and the eigenfrequency of the propeller in a similar oscillation mode. A frequency analysis was performed when the propeller was designed but this was not around the hinge and without the mass of the lug and bolts.

An alternative way to approximate the propeller mass was used. The propeller was expected to bend similar to a sine wave between the hinge and the roller and the tip was expected to remain straight. This shape is shown in Figure 8.4. The propeller mass distribution was the sum of the propeller blade, lug, and bolts which is shown in Figure 8.4. The propeller was sectioned into small sections with a local mass and a displacement compared to the displacement at the impact location. The local displacement was used to factor in both the relevant displacement compared to the impact location and the mechanical advantage compared to the impact location. If a location on the propeller only moves half compared to the impact location, it not only has to physically be displaced over half the distance but the impact location also has a factor 2 mechanical advantage. This means the local propeller mass was multiplied by the relevant displacement squared. This is shown in Figure 8.5. The sum of all the local effective masses was **0.713 kg**. This was used as the local propeller mass.

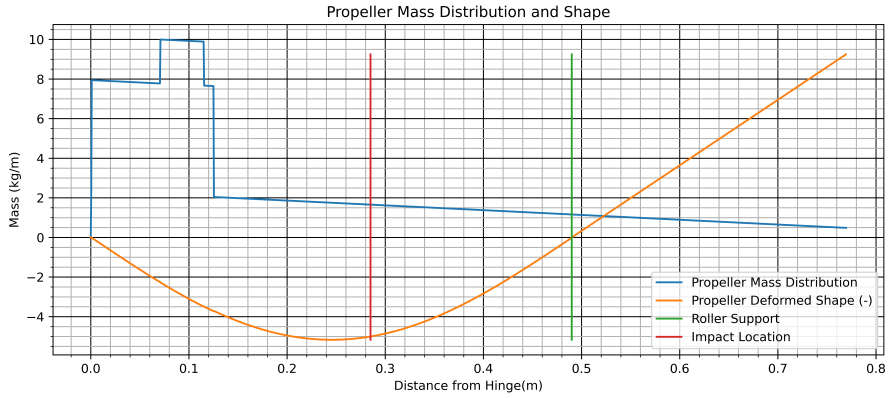

Figure 8.4: Propeller Mass Distribution and Shape

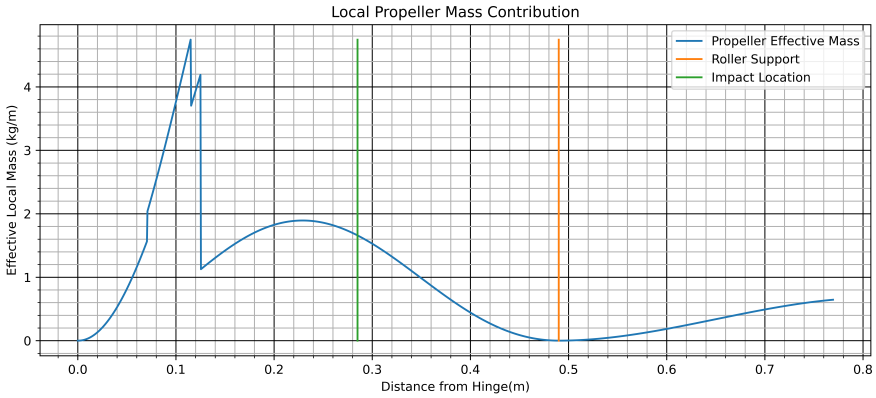

Figure 8.5: Propeller Effective Local Mass

8.2.2. Spring Constants

In section 6.4 and section 7.3 the spring rates for the coupons and propellers were calculated from the quasi-static tests. These spring rates were used as the basis for the contact stiffness and the propeller stiffness. The contact stiffness was taking directly from the coupon stiffness. The overall propeller stiffness already includes the contact stiffness as well. It can be seen as two springs in series. To get purely the propeller stiffness Equation 8.1 was used [78].

$$\frac{1}{k_{Tot}} = \frac{1}{k_1} + \frac{1}{k_2} \tag{8.1}$$

From subsection 2.3.1 it was clear that carbon composite structures in a high loading rate situation like an impact loading, react stiffer than in a low loading rate situation like the quasi-static test [21]. To determine the increase in stiffness, the quasi-static coupon tests were compared to the ASTM impact coupon tests.

A simple spring mass model was created with the spring constant from the quasi-static tests and the impactor mass. This model, shown in Figure 8.2, was compared to the results from the ASTM impact tests. This is shown in Figure 8.6. The difference in duration of the impact event was used to determine the increase in stiffness. It was found that when the spring constant in the model was multiplied by **1.47** the duration of the impact event was equal to the physical test. The model with the corrected spring constant is also shown in Figure 8.6. This multiplication factor was also applied to the propeller spring constant in the two mass model. It should be noted that this multiplication factor was determine while also taking into account the damping coefficient.

As mentioned in section 6.3 the correction factor was verified one more time in this section. For comparison, the uncorrected impact force history was compared to the single-mass model in Figure 8.7. Even though the spring constant was adjusted to match the impact duration the contact force was way of the single-mass model prediction. In Figure 8.6 the correction factor of 1.282 is already applied and the graphs match up. This supports the implementation of the correction factor determined in section 6.3.

8.2.3. Damping Coefficients

The damping coefficient parallel to the contact stiffness was estimated using the energy lost in the coupon impact tests by comparing the impact velocity to the rebound velocity. This exit velocity was then used to determine a damping coefficient with which the spring mass model from subsection 8.2.2 would have a matching exit velocity compared to the ASTM tests. The damping coefficient was found to be **790 Ns/m**. This coefficient was determined while also using the spring constant multiplication factor.

The damping coefficient for the propeller was however difficult to approximate. No information on the propeller response at high loading rates was known at this point. One way to approximate this damping coefficient would be to take the damping coefficient as the contact damping coefficient scaled using the

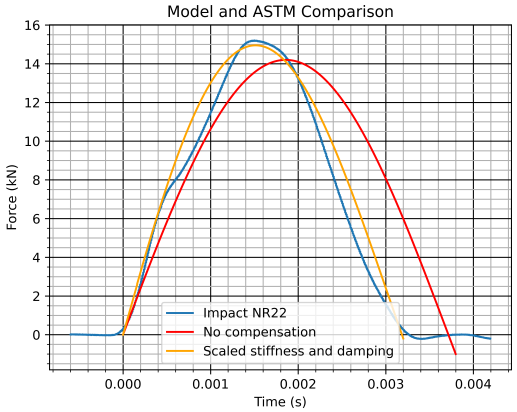

Figure 8.6: A Comparison between the Single mass model and the ASTM D7136 test results.

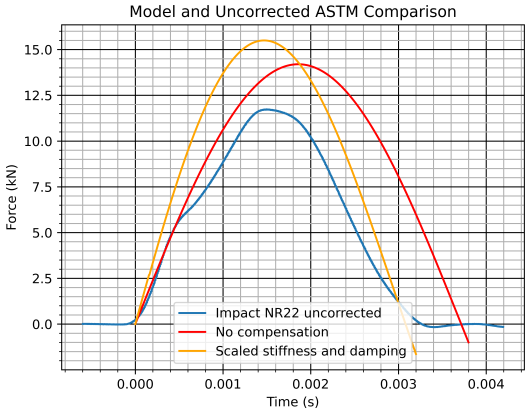

Figure 8.7: A Comparison between the Single mass model and the uncorrected ASTM D7136 test results.

difference in spring constant. This would be very inaccurate because a lot of factors are different including the materials and boundary conditions. The only information that resembles some form of damping that was available at this point was the hysteresis in the quasi-static tests. The hysteresis in the coupon tests was compared to the hysteresis in the propeller tests. This fraction was then used to scale the damping coefficient found for the contact. Although it was expected this damping coefficient was not very accurate it was the best guess at this stage in the process.

From Figure 7.5 it was clear that the amount of hysteresis in the propeller was scaled by the maximum load. That is why it was chosen to scale the hysteresis of the coupon tests shown in Figure 6.13 to 4kN by dividing it by 2. This was then compared to the hysteresis in the 4 kN load cycle shown in Figure 7.5. The scaled hysteresis in the coupons was 1.94 times higher than in the propeller. This is why a damping coefficient of **407 Ns/m** was chosen for the propeller. It should be noted that this value should be considered a guess. More information is needed to determine an accurate damping coefficient.

8.3. Results

The coefficients determined in the previous section were applied to the two mass model shown in Figure 8.1. The expected contact force plot of a 50 Joule impact on the propeller is shown in Figure 8.8 and a force prediction at 136 Joule is shown in Figure 8.9.

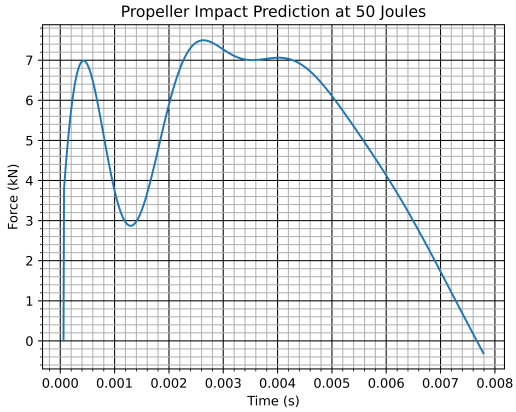

Figure 8.8: Prediction of the Contact Force at 50 Joule.

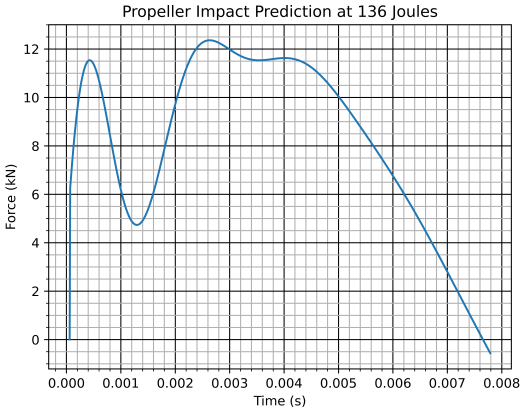

Figure 8.9: Prediction of the Contact Force at 136 Joule.

8.4. Discussion

The force prediction model would indicate that the damage threshold contact force determined in section 6.4 of 20 kN will not be reached before the 136 Joule upper threshold determined in chapter 4. This model indicated that an impact energy of 356 Joule is needed before 20 kN contact force is reached.

The two most uncertain coefficients in this chapter were the propeller stiffness multiplication factor and the propeller damping coefficient. Because these two values are uncertain a sensitivity analysis was performed to see what would happen when these values turn out to be incorrect. Increasing the propeller stiffness multiplication factor will increase the peak contact force. Decreasing the propeller damping coefficient will also increase the peak contact force. When the stiffness multiplication factor was increased to 1.7 and the damping coefficient was reduced to 200, the impact energy required to reach the 20 kN threshold is decreased to 274 Joule. This impact energy is still significantly higher than what is determined as the impact energy cut-off of 136 Joules in chapter 4. It was safe to assume that the BVID indentation threshold of 0.30 mm will not occur on the propeller in this location.

Even though it was expected that the damage threshold for BVID will not be reached during propeller impact testing, it was still useful to perform the propeller impact test. This test served as a validation of the model.

9

Propeller Impact Testing

The original goal of the propeller impact test was to create BVID on a PAL-V propeller. However, in chapter 8 it became apparent that the contact force expected during propeller impact testing will not be enough to cause BVID. This meant that this test had a new goal. The goal of the propeller impact test was to validate the model created in chapter 8 and determine its accuracy.

The test setup that was used for the propeller impact test along with the load cases is shown in section 9.1. The results of the test are explained in section 9.2. In section 9.3 the results and how these results validate the prediction model is discussed.

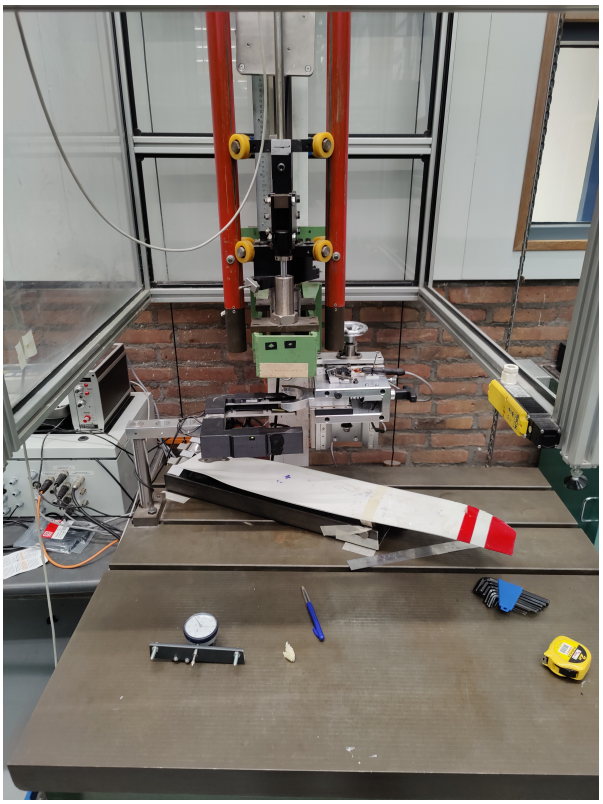

Figure 9.1: Propeller Impact Test Setup

9.1. Setup

For this test only the white propeller introduced in subsection 7.1.1 was used. The black propeller was not used for this test. After the white propeller tests were completed the drop tower stopped functioning and another day of testing did not fit the schedule. The propeller was placed inside the propeller fixture from subsection 7.1.2. The drop tower introduced in subsection 6.1.2 was used to apply the impact load. This test setup is shown in Figure 9.1

Load Cases

In section 8.4 it was predicted that the upper threshold for impact threats of 136 Joule will not be enough to cause BVID. Another limitation is the physical maximum impact that the drop tower that was used for these tests is capable of. In section 6.2 a maximum impact energy of 65.6 Joule was reached which seemed to be the maximum before the drop tower would start showing issues like not catching the dart or not recording the data. This propeller impact test started at a dart height of 0.5 meter. The drop height was increased to 1.2 meter for the second test. After this the drop height was increased until the drop tower was unable to function properly.

9.2. Results

Four propeller impact tests were performed. At an impact energy of 63 Joule, the drop tower was unable to catch the dart. This meant that the dart would hit the propeller multiple times. The fourth test was a step down to 55 Joule to see if the catch mechanism would function at this impact energy. During testing it was suspected that the data was not being recorded correctly on the third and fourth impact event because the catch mechanism was not being triggered. After analysing the data it seemed that the recorded data was the correct data from the main impact and not one of the smaller impacts caused by the dart not being captured. The results are shown in Figure 9.2,9.3,9.4 and 9.5 along with the model predictions. After these tests on the propeller no measurable indentation was found.

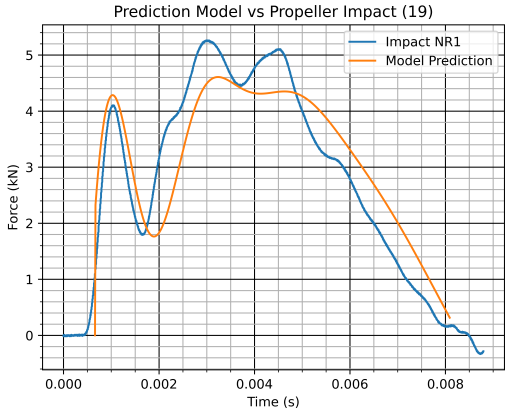

Figure 9.2: Force plot of First propeller impact with Model prediction. (19 Joule)

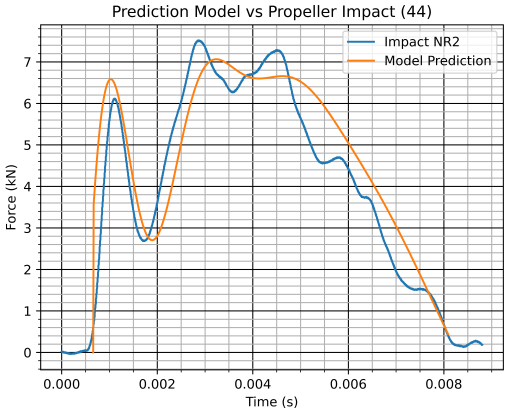

Figure 9.3: Force plot of Second propeller impact with Model prediction. (44 Joule)

9.3. Discussion

From the comparison plots of the prediction model and the propeller impact tests it can be seen that the model was able to predict the contact force to some degree. The impact tests and the model both have three distinct peaks after which the local contact oscillation was damped out. The magnitude of the peak was predicted within 13% of the true value. This section will however focus more on the differences.

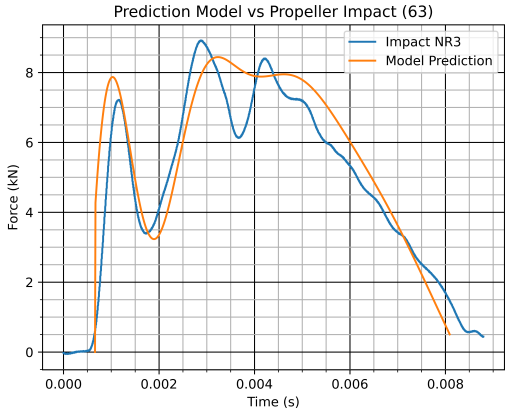

Figure 9.4: Force plot of Third propeller impact with Model prediction. (63 Joule)

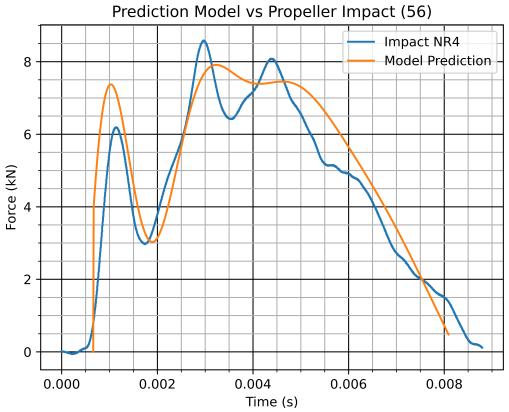

Figure 9.5: Force plot of Fourth propeller impact with Model prediction. (56 Joule)

The frequency of the contact oscillation seemed too slow in the model. This could be caused by the local propeller mass being lower than expected or the contact spring constant being higher than expected. A lower local mass could be caused by errors in the calculation method in subsection 8.2.1 or by the fact that the propeller is flexible and the shape predicted in subsection 8.2.1 is not the initial shape that the propeller followed. A higher contact spring constant could be caused by the edges of the propeller being closer to the impact location compared to the coupon fixture resulting in a small local plate and a higher spring constant. The higher spring constant could also be caused by the foam sandwich core that was present on the inside of the propeller.

The model also seemed to overestimate the initial spike in contact force. This would indicate that purely raising the contact spring constant would not have the desired response. This would increase the contact oscillation frequency but also the magnitude of the first peak. Probably a combination of reducing the local mass and increasing the contact stiffness would make the model more accurate.

Also visible from the propeller impact plots was that there are more oscillations present in the propeller. The model only considers two different oscillations but it was clear from the smaller peaks that this was not the case in the real situation. This was also clear in the high speed videos that were taken during the impact events. The oscillations visible in these videos are quite complex and will not be easily implemented in a simple model.

The damping in the model also seemed off. The second and third peak in the model showed that there was no significant oscillation remaining in the contact relation. The impact tests show however that there still was a local oscillation between the impactor and the propeller. Even though loading section of the model and the tests seem quite similar, the unloading was way steeper in the model compared to the tests. This would also indicate a significant difference in damping.

10 Conclusion

In this section it was evaluated to what extend the research goal was reached. The research goal was:

The goal of this research was to develop a method to inflict BVID to a carbon composite propeller blade which can be used for certification while minimizing the resources required.
From this research goal the following research question was formulated:

How can ASTM D7136 impact testing and quasi-static loading be used to predict the impact energy required to induce Barely Visible Impact Damage (BVID) for the certification of carbon composite propellers?

The following research sub-questions were formulated to answer the research question:

1. What are the requirements for impact damage to be considered BVID on the propeller for certification?
   (a) What are the impact threats for the propeller?
   (b) Where on the propeller should the impact damage be applied for certification?
   (c) What can be considered Barely Visible Impact Damage (BVID) on the propeller blade?
2. How do the results of ASTM D7136 testing correlate with the mechanical response of a similar coupon under quasi-static loading conditions?
3. How does the mechanical response of a coupon under quasi-static loading conditions correlate with the mechanical response of a propeller blade under similar loading conditions?
   (a) What are the boundary conditions on the propeller when the BVID is expected?
   (b) How can a clamping mechanism mimic these boundary conditions on the propeller during testing?
4. How can a prediction be made of the impact response of the propeller using coupon testing and propeller quasi-static testing?

In chapter 4 the impact threats were identified along with the critical impact location on the propeller. The impact energy expected has an upper threshold of 136 Joule. The most critical impact location is located on the back side of the propeller blade, 260 mm from the root of the propeller on the spar just before the transition into the skin. This answered sub-question 1(a) and 1(b). The probability of detection study performed in chapter 5 found that the detectability threshold for the PAL-V Liberty propeller is a dent depth of 0.30mm, answering sub-question 1(c). This means that for certification, impact needs to be applied at the critical location which results in a dent depth of at least 0.30 mm or until an impact energy of 136 Joule is reached. This dent depth is after relaxation. This relaxation was monitored but not enough data points were gathered to form an accurate prediction. It was estimated from the data that was gathered that the initial dent depth for BVID before relaxation is 0.38-0.40 mm.

After performing the ASTM D7136 impact tests and the quasi-static tests on the coupons in chapter 6, the results could be compared. The coupons seem to be able to support a higher load when subjected to impact loading compared to quasi-static loading. In chapter 8 this correlation was further explored. The coupons reacted stiffer when under impact loading compared to quasi-static loading. A multiplication factor of 1.47 had to be applied to the stiffness of the coupon to match the quasi-static stiffness to the impact stiffness. This provided the answer to sub-question 2.

To properly perform the tests on the propeller the boundary conditions had to be determined from which a clamping mechanism was designed. In subsection 7.1.2 the boundary conditions were identified as a hinged connection at the propeller lug with a roller support in the first vibration node. The roller support was placed at 490 mm from the hinge. The clamping mechanism designed to replicate these boundary conditions consisted of an aluminium block which would hold the propeller lug at the appropriate angle. The propeller was attached to the lug and a pin was placed underneath the propeller at 490 mm from the hinge on which the propeller was supported. Sub-questions 3(a) and 3(b) were answered resulting in the propeller test fixture.

Question 3 aimed to identify the differences between the coupon and propeller quasi-static tests in order to apply this knowledge in a predictive model. The difference was mainly characterised by the difference in stiffness in the structural reaction of the coupons compared to the propeller. The spring constant of the propeller was 596 kN/m and the spring constant of the coupon was 3520 kN/m.

It was found that a prediction can be made of the impact response of the propeller by creating a two-mass, spring and damper system. The coefficients needed in this model were taken from the coupon tests and the propeller quasi-static tests. This answered sub-question 4.

This research has proven that ASTM D7136 impact testing and quasi-static loading can predict the contact force encountered in an impact event on a carbon composite propeller. This prediction was done by using a two-mass spring and damper model. The parameters used in the model were determined by ASTM D7136 and quasi-static testing.

A prediction of the impact energy required to induce barely visible impact damage was done. This impact energy was 356 Joule. Unfortunately it was not possible to validate this prediction as this energy level was too high for the equipment available. The method does however show potential that this is possible if the impact energy necessary is withing the capabilities of the test equipment and within the impact energy range determined for certification.

The model was able to predict the contact force to within 13 % of the value found during testing. This is in the same range as the different contact forces found during ASTM D7136 impact testing for impacts with similar damage. To know for sure if this method can be used to predict BVID energy levels, it has to be applied in a different situation were BVID is actually possible. The model was however able to predict that BVID would not be found in this situation before any actual propeller impact tests had to be performed.

Even though there is room for improvement for this model, the accuracy is high enough to predict the contact forces to within the variation found between similar impact tests. This proves that these simple physical tests and simple models are able to predict the impact event. When comparing the simplicity of this method to FEA models it shows that when a problem is divided into simpler, smaller steps, a solution can be found.

11

Recommendations

Unfortunately, the predicted energy for BVID at the critical impact location was too high to be validated. A validation of the model at BVID levels would be very valuable. A composite part which would have BVID at a lower contact force with a relatively high overall stiffness will be more suited to reach BVID indentation. This can for example be a composite body panel with a carbon fiber sandwich structure with a relatively thin skin. The main reason for the high contact force required for BVID in the propeller is the very high material thickness in the propeller spar.

One thing that could also be improved is the simulation of the damping in the model. The prediction of the propeller damping as done in subsection 8.2.3 has not been supported by tests or previous research. Research into how this damping works, and how to determine the relevant coefficients can improve the accuracy of the model.

In this research project the switch was made to prediction the contact force instead of the dent depth from a certain impact event. Even though it is discovered that a certain contact force is required to initiate a significant dent depth it is not yet determined what exactly needs to happen after this threshold to create a certain dent depth after the knee point. It was fortunate that the knee point correlated with the BVID threshold. If the knee point would have been lower, the dent depth progression after the knee point has to be known to predict the impact energy for BVID.

Because the BVID damage was not encountered in the proposed location on the propeller, PAL-V has a few options for demonstrating the impact damage resistance of the propeller. A new location can be selected where the material is thinner or the boundary conditions are stiffer. Another option would be to apply a 136 Joule impact at the proposed location. This could still produce internal damage without leaving a dent that is still considered BVID. Another option would be to try using higher impact velocities this would lead to the BVID dent to occur at a lower energy level as the local mass of the propeller starts to play a bigger role.

The data from this research can also be expanded to different coupon thicknesses. This will result in a prediction of the BVID contact force on a wide range of material thickness. This can be used to predict BVID on different parts of the propeller or different components on the PAL-V Liberty. With this information the coupon tests don't have to be performed every time BVID has to be applied to a new component. This would mean that, if this variable thickness coupon data is known, only quasi-static tests need to be performed on the component to predict the BVID impact energy level.

One last recommendation is that the relaxation has to be mapped more accurately. The most accurate way would be to perform the relaxation measurements more consistently on a new set of coupons. But even measuring the indentation depth on the coupons created for this research in the coming months will make the relaxation prediction more accurate.

Bibliography

[1] *Composite Materials Handbook Volume 3 Chapter 12: Damage Resistance, Durability, and Damage Tolerance*. Volume 3. SAE International on behalf of CMH-17, a division of Wichita State University, 2012. ISBN: 978-0-7680-7813-8.

[2] *Development and certification of composite propellers - mcfarlane aviation*. URL: https://www.mcfarlaneaviation.com/media/documents/development-and-certification-of-composite-propellers.pdf (visited on 07/14/2023).

[3] W. J. Stronge. *Impact mechanics*. Cambridge University Press, 2000.

[4] D. Mohotti, M. Ali, T. Ngo, J. Lu, P. Mendis, and D. Ruan. "Out-of-plane impact resistance of aluminium plates subjected to low velocity impacts". In: *Materials & Design* 50 (Sept. 2013), pp. 413–426. ISSN: 0261-3069. DOI: 10.1016/J.MATDES.2013.03.023.

[5] W. J. Cantwell and j Morton. "The impact resistance of composite materials-a review". In: *Composites* 22 (5 1991), pp. 347–362.

[6] EASA. *CS-27 Certification Specifications, Acceptable Means of Compliance and Guidance Material for Small Rotorcraft*. 2021.

[7] EASA. *SC-GYRO-1 SPECIAL CONDITION for Gyroplane - Road Vehicle Use*. 2021.

[8] EASA. *CS-P Certification Specifications and Acceptable Means of Compliance for Propellers (Amendment 2)*. 2020.

[9] EASA. *AMC 20-29 Acceptable Means of Compliance for Certification of Composite Aircraft Structures*. 2010.

[10] J. Rouchon. *Fatigue and Damage Tolerance Evaluation of Structures: The Composite Materials Response*. NLR, May 2009.

[11] H. Kan, R. Cordero, and R. Whitehead. *Advanced Certification Methodology for Composite Structures*. Naval Air Warfare Center, Apr. 1997.

[12] *Carbon-fibre-reinforced plastics — Determination of compression-after-impact properties at a specified impact-energy level*. International Organization for Standardization, Aug. 2009.

[13] P. F. R. Massart. "Modelling Impact Damage on Aircraft Structures (MIDAS) Predicting impact damage on (composite) aircraft based on maintenance data of (metal) aircraft". MSc Thesis. 2018.

[14] S. Dubinskii, V. Senik, and Y. Feygenbaum. "The Significance of In-Service Factors for the Visual Detectability of Impact Damage in Composite Airframe". In: *Journal of Nondestructive Evaluation* 38 (4 Dec. 2019). ISSN: 15734862. DOI: 10.1007/s10921-019-0632-3.

[15] F. JIANG, Z. GUAN, Z. LI, and X. WANG. "A method of predicting visual detectability of low-velocity impact damage in composite structures based on logistic regression model". In: *Chinese Journal of Aeronautics* 34 (1 Jan. 2021), pp. 296–308. ISSN: 10009361. DOI: 10.1016/j.cja.2020.10.006.

[16] L. Cook. "Visual Inspection Reliability for Composite Aircraft Structures". PhD thesis. Cranfield University, 2009.

[17] E. Bakker. "Development of a Damage Tolerance Certification Methodology for Composite Structures". MSc Thesis. TU Delft, 2013.

[18] R. Talreja and N. Phan. "Assessment of damage tolerance approaches for composite aircraft with focus on barely visible impact damage". In: *Composite Structures* 219 (July 2019), pp. 1–7. ISSN: 02638223. DOI: 10.1016/j.compstruct.2019.03.052.

[19] S. Abrate. *Impact engineering of composite structures*. Springer, 2011, 1 online resource. ISBN: 9783709105238.

[20] R. W. Clough and J. Penzien. *DYNAMICS OF STRUCTURES*. Third Edition. Computers and Structures Inc., 2003.

[21] H. AL-Zubaidy, X. L. Zhao, and R. Al-Mihaidi. “Mechanical behaviour of normal modulus carbon fibre reinforced polymer (CFRP) and epoxy under impact tensile loads”. In: *Procedia Engineering* 10 (2011), pp. 2453–2458. ISSN: 18777058. DOI: 10.1016/j.proeng.2011.04.404.

[22] G. A. Schoeppner and S. Abrate. “Delamination threshold loads for low velocity impact on composite laminates”. In: *Composites Part A: Applied Science and Manufacturing* 31 (9 2000), pp. 903–915. ISSN: 1359835X. DOI: 10.1016/S1359-835X(00)00061-0.

[23] R. Olsson. “Analytical prediction of damage due to large mass impact on thin ply composites”. In: *Composites Part A: Applied Science and Manufacturing* 72 (Feb. 2015). DOI: 10.1016/j.compositesa.2015.02.005.

[24] W. He, Z. Guan, X. Li, and D. Liu. “Prediction of permanent indentation due to impact on laminated composites based on an elasto-plastic model incorporating fiber failure”. In: *Composite Structures* 96 (Feb. 2013), pp. 232–242. ISSN: 02638223. DOI: 10.1016/j.compstruct.2012.08.054.

[25] N. TAKEDA, S. MINAKUCHI, and Y. OKABE. “Smart Composite Sandwich Structures for Future Aerospace Application -Damage Detection and Suppression-: a Review”. In: *Journal of Solid Mechanics and Materials Engineering* 1 (1 2007), pp. 3–17. DOI: 10.1299/jmmp.1.3.

[26] J. Komorowski, R. Gould, and A. O. Marincak. *Study of the effect of time and load on impact damage visibility*. Canadian international composites conference and exhibition, Sept. 1993, pp. 441–446.

[27] G. A. Davies and R. Olsson. “Impact on composite structures”. In: *Aeronautical Journal* 108 (1089 2004), pp. 541–563. ISSN: 00019240. DOI: 10.1017/S0001924000000385.

[28] C. Kassapoglou. *Modeling the Effect of Damage in Composite Structures : Simplified Approaches.* Wiley, 2015, p. 484. ISBN: 9781119013235.

[29] L. Carlsson and G. Kardomateas. *Structural and Failure Mechanics of Sandwich Composites*. 1st ed. Vol. 1. Springer, May 2011. ISBN: 978-1-4020-3224-0. DOI: 10.1007/978-1-4020-3225-7.

[30] N. Razali, M. Sultan, F. Mustapha, N. Yidris, and M. Ishak. “Impact Damage on Composite Structures-A Review”. In: *The International Journal Of Engineering And Science* 3 (7 2014), pp. 08–20.

[31] W. J. Cantwell and J. Morton. “Comparison of the low and high velocity Impact response of CFRP”. In: *Composites* 20 (6 Nov. 1989).

[32] N. van Hoorn, C. Kassapoglou, S. Turteltaub, and W. van den Brink. “Experimental damage tolerance evaluation of thick fabric carbon/epoxy laminates under low-velocity and high-velocity impact and compression-after-impact”. In: *Journal of Composite Materials* 56 (5 Mar. 2022), pp. 761–778. ISSN: 1530793X. DOI: 10.1177/00219983211060501.

[33] M. S. Rajput, M. Burman, F. Forsberg, and S. Hallström. “Experimental and numerical study of the response to various impact energy levels for composite sandwich plates with different face thicknesses”. In: *Journal of Sandwich Structures and Materials* 21 (5 June 2019), pp. 1654–1682. ISSN: 15307972. DOI: 10.1177/1099636219837133.

[34] M. D. Robb, W. S. Arnold, and I. H. Marshall. “The damage tolerance of GRP laminates under biaxial prestress”. In: *Composite Structures* 32 (1995). No difference at low strain, pp. 141–149.

[35] B. Whittingham, I. H. Marshall, T. Mitrevski, and R. Jones. “The response of composite structures with pre-stress subject to low velocity impact damage”. In: *Composite Structures* 66 (1-4 Oct. 2004), pp. 685–698. ISSN: 02638223. DOI: 10.1016/j.compstruct.2004.06.015.

[36] D. Zheng and W. K. Binienda. “Analysis of Impact Response of Composite Laminates under Prestress”. In: *JOURNAL OF AEROSPACE ENGINEERING* 21 (4 2008), pp. 197–205. DOI: 10.1061/ASCE0893-1321200821:4197.

[37] N. Guillaud, C. Froustey, F. Dau, and P. Viot. “Impact response of thick composite plates under uniaxial tensile preloading”. In: *Composite Structures* 121 (Mar. 2015), pp. 172–181. ISSN: 02638223. DOI: 10.1016/j.compstruct.2014.11.021.

[38] Y. Hu, Y. Shi, D. Liu, and J. Zhang. “Low-velocity impact damage tolerance of ultrahigh molecular weight polyethylene/carbon fiber laminates under prestress”. In: *Polymer Composites* 43 (2 Feb. 2022), pp. 712–729. ISSN: 15480569. DOI: 10.1002/pc.26404.

[39] R. Panciroli, M. Ahmadi, M. Fotouhi, and G. Minak. *Dynamic Deformation, Damage and Fracture in Composite Materials and Structures: Chapter 5, Low-velocity impact on preloaded and curved laminates*. Elsevier, 2023, pp. 121–140. ISBN: 9780128239797. DOI: 10.1016/b978-0-12-823979-7.00006-5.

[40] F. Esrail and C. Kassapoglou. “An efficient approach for damage quantification in quasi-isotropic composite laminates under low speed impact”. In: *Composites Part B: Engineering* 61 (May 2014), pp. 116–126. ISSN: 13598368. DOI: 10.1016/j.compositesb.2014.01.033.

[41] K. N. Shivakumar, W. Elber, and W. Illg. “Prediction of Impact Force and Duration Due to Low-Velocity Impact on Circular Composite Laminates”. In: *Journal of Applied Mechanics* 52 (Sept. 1985), pp. 674–680.

[42] E. H. Lee. “The Impact of a Mass Striking a Beam”. In: *Journal of Applied Mechanics* 7 (4 Dec. 1940), A129–A138. ISSN: 0021-8936. DOI: 10.1115/1.4009061.

[43] R. Olsson. “Closed form prediction of peak load and delamination onset under small mass impact”. In: *Composite Sructures* 59 (2003), pp. 341–349.

[44] C. Bouvet, S. Rivallant, and J. J. Barrau. “Modelling of impact damage and permanent indentation on laminate composite plate”. In: *ECCM14 - 14th European Conference on Composite Materials* (June 2010).

[45] C. Bouvet, S. Rivallant, and J.-J. Barrau. “Low velocity impact modeling in composite laminates capturing permanent indentation”. In: *Composites Science and Technology* 72 (16 2012), pp. 1977–1988. ISSN: 0266-3538. DOI: 10.1016/j.compscitech.2012.08.019i.

[46] *ASTM D7136 - Standard Test Method for Measuring the Damage Resistance of a Fiber-Reinforced Polymer Matrix Composite to a Drop-Weight Impact Event*. American Society for Testing and Materials, 2012. DOI: 10.1520/D7136_D7136M-12.

[47] M. R. Condruz, A. Paraschiv, I. S. Vintilă, M. Sima, A. Deutschlander, and F. Dumitru. “Evaluation of low velocity impact response of carbon fiber reinforced composites”. In: vol. 779 KEM. Trans Tech Publications Ltd, 2018, pp. 3–10. ISBN: 9783035712780. DOI: 10.4028/www.scientific.net/KEM.779.3.

[48] D. D. Vito, T. Pärnänen, J. Jokinen, O. Orell, and M. Kanerva. *Lateral indentation and impact analyses on curved composite shells*. Laboratory of Materials Science, Tampere University of Technology, 2020.

[49] G. Minak and D. Ghelli. “Influence of diameter and boundary conditions on low velocity impact response of CFRP circular laminated plates”. In: *Composites Part B: Engineering* 39 (6 Sept. 2008), pp. 962–972. ISSN: 13598368. DOI: 10.1016/j.compositesb.2008.01.001.

[50] K. R. Kaware and M. S. Kotambkar. “Effect of Impactor velocity and boundary condition on low velocity impact finite element modelling of CFRP composite laminates”. In: vol. 1004. IOP Publishing Ltd, Dec. 2020. DOI: 10.1088/1757-899X/1004/1/012018.

[51] A. M. Amaro, P. N. Reis, A. G. Magalhães, and M. F. D. Moura. “The influence of the boundary conditions on low-velocity impact composite damage”. In: *Strain* 47 (SUPPL. 1 June 2011). ISSN: 00392103. DOI: 10.1111/j.1475-1305.2008.00534.x.

[52] W. Richardson and M. J. Wisheart. “Review of low-velocity impact properties of composite materials”. In: *Composites Part A* 27 (A 1996), pp. 1123–1131.

[53] S. M. Lee and P. Zahuta. “Instrumented Impact and Static Indentation of Composites”. In: *Journal of Composite Materials* 25 (2 1991), pp. 204–222. DOI: 10.1177/002199839102500205.

[54] E. Wu and K. Shyu. “Response of Composite Laminates to Contact Loads and Relationship to Low-Velocity Impact”. In: *Journal of Composite Materials* 27 (15 1993), pp. 1443–1464. DOI: 10.1177/002199839302701502.

[55] G. Belingardi and R. Vadori. “Influence of the laminate thickness in low velocity impact behavior of composite material plate”. In: *Composite Structures* 61 (2 2003), pp. 27–38. ISSN: 02638223. DOI: 10.1016/S0263-8223(03)00027-8.

[56] A. L. Highsmith. *A Study of the Use of Contact Loading to Simulate Low Velocity Impact*. Department of Aerospace Engineering, The University of Alabama, 1997.

[57] C. Breen, F. Guild, and M. Pavier. “Impact of thick CFRP laminates: The effect of impact velocity”. In: *Composites Part A: Applied Science and Manufacturing* 36 (2 2005), pp. 205–211. ISSN: 1359835X. DOI: 10.1016/j.compositesa.2004.06.005.

[58] B. D. Lawrence and R. P. Emerson. *A Comparison of Low-Velocity Impact and Quasi-Static Indentation*. Army Research Laboratory, 2012.

[59] S. W. Spronk, M. Kersemans, J. C. D. Baerdemaeker, F. A. Gilabert, R. D. Sevenois, D. Garoz, C. Kassapoglou, and W. V. Paepegem. “Comparing damage from low-velocity impact and quasi-static indentation in automotive carbon/epoxy and glass/polyamide-6 laminates”. In: *Polymer Testing* 65 (Feb. 2018), pp. 231–241. ISSN: 01429418. DOI: 10.1016/j.polymertesting.2017.11.023.

[60] M. P. Delaney, S. Y. Fung, and H. Kim. “Dent depth visibility versus delamination damage for impact of composite panels by tips of varying radius”. In: *Journal of Composite Materials* 52 (19 Aug. 2018), pp. 2691–2705. ISSN: 1530793X. DOI: 10.1177/0021998317752502.

[61] Z. Shen, Y. G. Xu, and A. Chrysanthou. “Correlation of dent depth to maximum contact force and damage of composite laminates”. In: vol. 627. Trans Tech Publications Ltd, 2015, pp. 353–356. DOI: 10.4028/www.scientific.net/KEM.627.353.

[62] M. Rausand. *Risk assessment : theory, methods, and applications*. J. Wiley & Sons, 2011. ISBN: 9781118626085.

[63] S. I. Thorsson, S. P. Sringeri, A. M. Waas, B. P. Justusson, and M. Rassaian. “Experimental investigation of composite laminates subject to low-velocity edge-on impact and compression after impact”. In: *Composite Structures* 186 (Feb. 2018), pp. 335–346. ISSN: 02638223. DOI: 10.1016/j.compstruct.2017.11.084.

[64] T. Gordon, X. Xu, M. R. Wisnom, S. R. Hallett, and B. C. Kim. “Improved impact damage resistance of tapered composite laminates using a ply scarfing technique”. In: *Composites Part A: Applied Science and Manufacturing* 166 (Mar. 2023). ISSN: 1359835X. DOI: 10.1016/j.compositesa.2022.107391.

[65] E. Herricks, D. Mayer, and S. Majumdar. *Foreign Object Debris Characterization at a Large International Airport*. Center of Excellence for Airport Technology, Feb. 2015.

[66] R. K. Schmidt. *The Design of Aircraft Landing Gear*. SAE International, 2021. ISBN: 9780768099430.

[67] S. N. Nguyen, E. S. Greenhalgh, J. M. R. Graham, A. Francis, R. Olsson, S. Sicomp, and M. Sweden. “Runway debris impact threat maps for transport aircraft”. In: *The Aeronautical Journal* 118 (2014). DOI: 10.1017/S0001924000009106.

[68] H. Park. “A study on impact damage analysis of composite propeller blade of turboprop aircraft”. In: *Key Engineering Materials* 577-578 (2014), pp. 489–492. ISSN: 16629795. DOI: 10.4028/www.scientific.net/KEM.577-578.489.

[69] EASA. *Easy Access Rules for Standardised European Rules of the Air (SERA) - Revision from March 2022*. 2022.

[70] D. van Putten and H. de Moel. *A hail climatology of the Netherlands*. 2019.

[71] H. P. Böhm. “A General Equation for the Terminal Fall Speed of Solid Hydrometeors.” In: *Journal of Atmospheric Sciences* 46 (15 1989), pp. 2419–2427. ISSN: 0022-4928. DOI: 10.1175/1520-0469(1989)046.

[72] CBS. *Victims of frequently occurring crime*. Mar. 2005. URL: https://opendata.cbs.nl/#/CBS/en/dataset/37685ENG/table?searchKeywords=vandalism (visited on 07/14/2023).

[73] UNSW. *Smashing bricks and golf balls: more collision examplesfrom Physclips*. URL: https://www.animations.physics.unsw.edu.au/jw/smashing-bricks.html (visited on 07/14/2023).

[74] L. Keith. *Advisory Circular 25.1309-1A*. Federal Aviation Administration, 1988.

[75] S. Dubinskii, Y. Feygenbaum, V. Senik, and E. Metelkin. “A study of accidental impact scenarios for composite wing damage tolerance evaluation”. In: *Aeronautical Journal* 123 (1268 Oct. 2019), pp. 1724–1739. ISSN: 00019240. DOI: 10.1017/aer.2018.152.

[76] L. Cook, A. Boulic, and D. Harris. *Reliability of damage detection in advanced composite aircraft structures : prepared for CAA by*. TSO, 2013. ISBN: 9780117927285.

[77] *Instron 5989 universial testing system*. URL: https://www.instron.com/en/products/testing-systems/universal-testing-systems/high-force-universal-testing-systems/5989-floor-model (visited on 08/29/2023).

[78] K. R. Symon. *Mechanics*. 3d. Addison-Wesley, 1971, p. 639.

A

ASTM D7136 Coupon Impact Data

Table A.1: ASTM D7136 coupon impact data

Impact Number	**Coupon Quality**	Impact Energy (Joule)	Indentation (mm)
1	3	44.11	0.20
2	2	35.97	0.10
3	3	44.92	0.25
4	2	59.96	0.6
5	2	44.92	0.22
6	1	48.95	0.30
7	1	51.63	0.35
8	3	62.36	0.95
9	3	57.70	0.6
10	1	52.57	0.37
11	1	55.56	0.38
12	1	53.54	0.53
13	1	49.82	0.28
14	1	48.95	0.25
15	1	50.71	0.33
16	1	56.62	0.41
17	1	50.71	0.30
18	2	58.81	0.58
19	1	56.62	0.35
20	2	61.14	0.80
21	3	28.61	0.25
22	2	28.19	0.23
23	2	27.81	0.17
24	1	28.19	0.23
25	3	56.01	0.45
26	2	65.63	0.63
27	2	65.63	1.05
28	1	63.00	0.58
29	2	67.00	1.10

B

ANSYS Analysis Illustrations

In this appendix the strength and deformation analysis of the propeller fixture is provided. Figure B.1 shows the loadcase on the fixture when supported on the compression test bench. In Figure B.2 the deformation in the vertical direction of this propeller fixture is shown with a scaling factor of 79 to visualize the deformation. The maximum deformation found in the vertical direction is 0.15 mm. The internal stresses in the aluminium block and the roller pin holes are shown in Figure B.3 and Figure B.4. Both stress values are well below the yield strength of the steel and aluminium used.

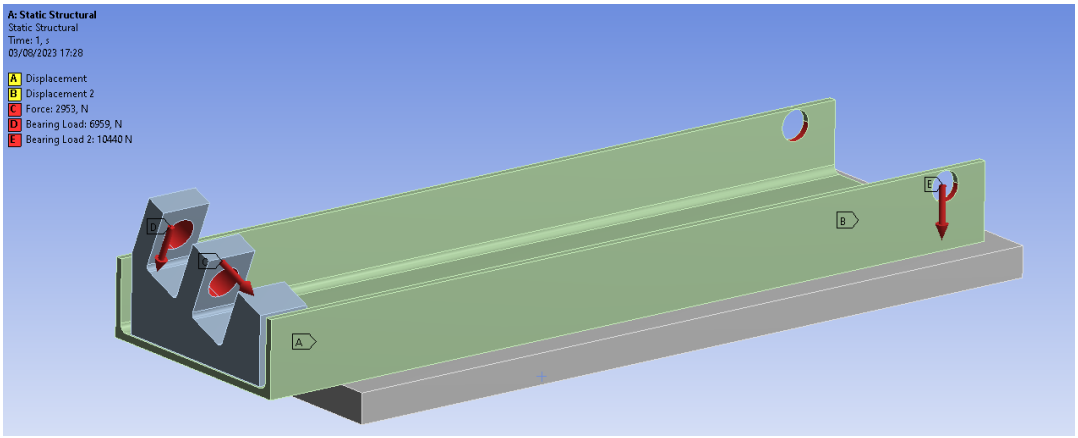

Figure B.1: ANSYS loadcase for the Propeller Fixture Analysis

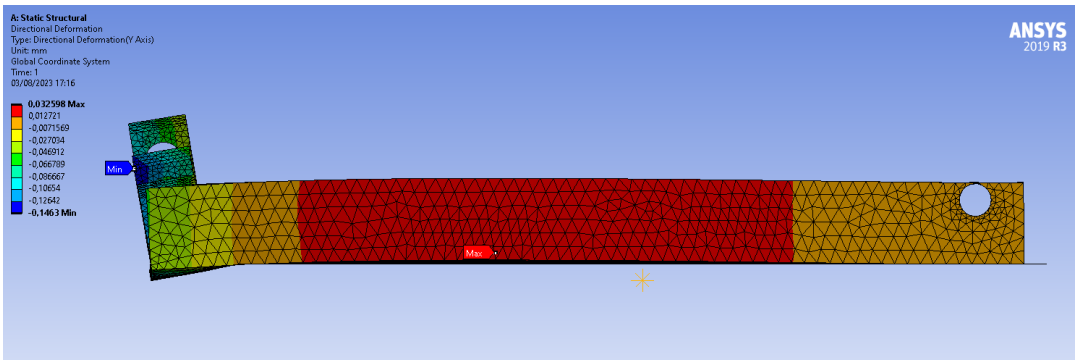

Figure B.2: Deformation in the Vertical Direction.

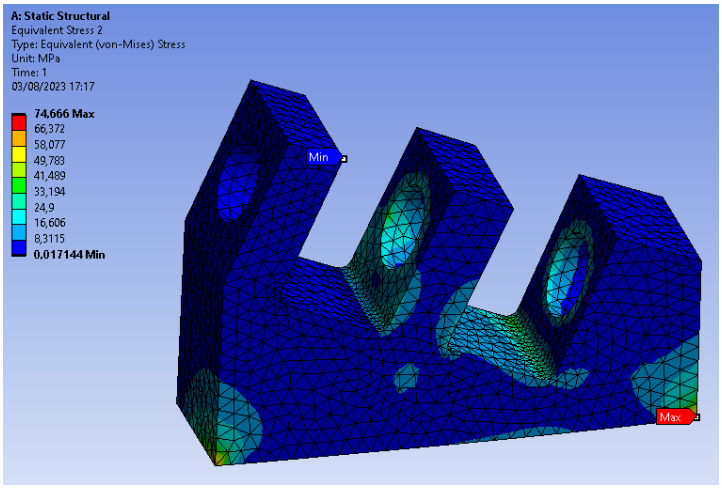

Figure B.3: The Equivalent stress in the Aluminium block.

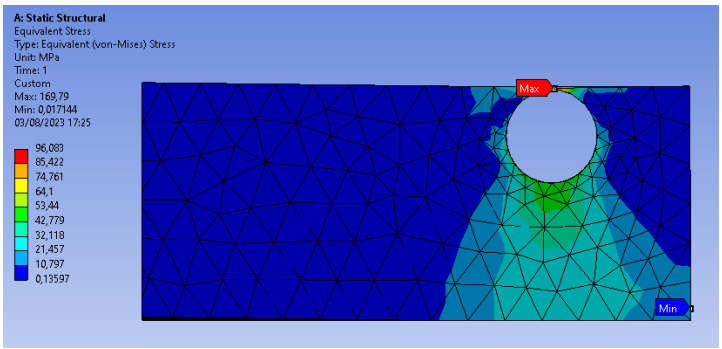

Figure B.4: The Equivalent stress in at the Roller pin holes.